

Ultrahigh and Selective SO₂ Uptake in Inorganic Anion-Pillared Hybrid Porous Materials

Xili Cui, Qiwei Yang,* Lifeng Yang, Rajamani Krishna, Zhiguo Zhang, Zongbi Bao, Hui Wu, Qilong Ren, Wei Zhou, Banglin Chen,* and Huabin Xing*

The efficient capture of SO₂ is of great significance in gas-purification processes including flue-gas desulfurization and natural-gas purification, but the design of porous materials with high adsorption capacity and selectivity of SO₂ remains very challenging. Herein, the selective recognition and dense packing of SO₂ clusters through multiple synergistic host–guest and guest–guest interactions by controlling the pore chemistry and size in inorganic anion (SiF₆^{2−}, SIFSIX) pillared metal–organic frameworks is reported. The binding sites of anions and aromatic rings in SIFSIX materials grasp every atom of SO₂ firmly via S^{δ+}...F^{δ−} electrostatic interactions and O^{δ−}...H^{δ+} dipole–dipole interactions, while the guest–guest interactions between SO₂ molecules further promote gas trapping within the pore space, which is elucidated by first-principles density functional theory calculations and powder X-ray diffraction experiments. These interactions afford new benchmarks for the highly efficient removal of SO₂ from other gases, even if at a very low SO₂ concentration. Exceptionally high SO₂ capacity of 11.01 mmol g^{−1} is achieved at atmosphere pressure by SIFSIX-1-Cu, and unprecedented low-pressure SO₂ capacity is obtained in SIFSIX-2-Cu-i (4.16 mmol g^{−1} SO₂ at 0.01 bar and 2.31 mmol g^{−1} at 0.002 bar). More importantly, record SO₂/CO₂ selectivity (86–89) and excellent SO₂/N₂ selectivity (1285–3145) are also achieved. Experimental breakthrough curves further demonstrate the excellent performance of these hybrid porous materials in removing low-concentration SO₂.

Rapid economic growth all over the world has resulted in the excessive energy consumption as well as increasing environmental burdens.^[1,2] One of the most serious related problems is the emission of sulfur dioxide (SO₂), induced by the utilization


of low-grade fossil fuels.^[3–6] Besides the direct detriment on environment and human health, SO₂ will significantly inactivate the adsorbents or absorbents in removing CO₂ from flue gas although the concentration of SO₂ in flue gas is very low (cat. 2000 ppm).^[7,8] Moreover, in the reactions such as selective catalytic reduction of NO_x and catalytic combustion of CH₄,^[9,10] even trace amount of SO₂ could poison the catalysts and this deactivation is irreversible. The traditional flue-gas desulfurization (FGD) processes, with limestone or organic solvents as the absorbents,^[11,12] can remove about 90–95% SO₂. However, these FGD technologies are energy-intensive and not efficient for the deep desulfurization. Therefore, there is an urgent demand for efficient technology to remove trace SO₂ in flue gas and other SO₂-containing gases.

In the past decades, the development of energy-efficient physical-adsorption separation technology shows great potential in gas separation, which greatly motivates the design and synthesis of highly efficient porous materials.^[13–15] Metal–organic frameworks (MOFs) and/or porous coordination polymers are

a class of hybrid porous materials composed of metal units joined by organic/inorganic linkers, in which the diversity of the organic/inorganic linkers and exquisite control over pore aperture size promise great potential for gas separation and purification.^[16–18] However, compared to the separation of CO₂

Dr. X. L. Cui, Dr. Q. W. Yang, L. F. Yang, Dr. Z. G. Zhang, Dr. Z. B. Bao, Prof. Q. L. Ren, Prof. H. B. Xing
Key Laboratory of Biomass Chemical Engineering
of Ministry of Education
College of Chemical and Biological Engineering
Zhejiang University
Hangzhou 310027, China
E-mail: yangqw@zju.edu.cn; xinghb@zju.edu.cn
Prof. R. Krishna
Van't Hoff Institute for Molecular Sciences
University of Amsterdam
Science Park 904, Amsterdam 1098 XH, The Netherlands

Dr. H. Wu, Prof. W. Zhou
Center for Neutron Research
National Institute of Standards and Technology
Gaithersburg, MD 20899-6102, USA
Prof. B. L. Chen
Department of Chemistry
University of Texas at San Antonio
One UTSA Circle
San Antonio, TX 78249-0698, USA
E-mail: banglin.chen@utsa.edu

 The ORCID identification number(s) for the author(s) of this article can be found under <https://doi.org/10.1002/adma.201606929>.

DOI: 10.1002/adma.201606929

and hydrocarbons,^[19–29] the selective adsorption of SO₂ has rarely been studied on MOFs, especially the adsorption at low partial pressures that is actually needed by the gas desulfurization.^[30–36] Generally, the desulfurization of flue gas is a step before CO₂ scrubbing process, however, few work paid attention to the selective removal of SO₂ from CO₂. In fact, considering the acidic nature of both SO₂ and CO₂ molecules and the much lower SO₂ concentration in flue gas than CO₂ (CO₂: 10–12%, v/v; SO₂: about 2000 ppm), it is very challenging to remove SO₂ from CO₂ with high selectivity.^[37,38] These abovementioned problems prompted us to develop advanced porous materials with delicate structure and chemistry for the adsorption of SO₂, and elucidate the way in which contributions such as pore size and pore surface electrostatic environment enhance the selective recognition of SO₂ with high uptake capacity.

In this work, we for the first time reported the selective recognition and dense packing of the so-called “SO₂ cluster” using hybrid porous materials through precisely tuning the pore size and pore chemistry. Featuring copper coordination networks with inorganic hexafluorosilicate (SiF₆^{2−}, SIFSIX) anions and organic linkers, SIFSIX-1-Cu (1 = 4,4′-bipyridine)^[24] and SIFSIX-2-Cu-i (2 = 4,4′-dipyridylacetylene, i = interpenetrated)^[19] contain pore spaces that enable high SO₂ uptake with specific recognition and afford new benchmarks for the highly efficient removal of SO₂ from other gases. Not only extraordinary ambient uptake of SO₂ was achieved with SIFSIX-1-Cu as adsorbent, but also unprecedented low-pressure SO₂ capacity was attained with SIFSIX-2-Cu-i. Moreover, record SO₂/CO₂ selectivity and excellent SO₂/N₂ selectivity were also exhibited by the SIFSIX materials. We attribute this exceptional performance to the synergistic guest–host interactions (S^{δ+}...F^{δ−} and O^{δ−}...H^{δ+} interactions) that firmly grasp every atom of SO₂ in the pores of SIFSIX materials along with the considerable guest–guest interactions among SO₂ molecules and the optimal

pore size, which together enable the preferential binding and cluster formation of SO₂ in the pores densely.

These SIFSIX materials exhibit a pillared square-grid 3D structure with inorganic SiF₆^{2−} ions as a linear bridge between transition-metal moieties. Previously, we have succeeded in the specific recognition of acetylene from ethylene using SIFSIX materials.^[39] In this work, we systematically studied the adsorption of SO₂ on SIFSIX-1-Cu, SIFSIX-2-Cu (2, 4,4′-dipyridylacetylene), SIFSIX-2-Cu-i, SIFSIX-3-Zn (3,pyrazine), and SIFSIX-3-Ni at atmospheric and low pressures. At first, the uptake capacity of SO₂ as single-component gas on activated SIFSIX-1-Cu, SIFSIX-2-Cu, SIFSIX-2-Cu-i, SIFSIX-3-Zn, and SIFSIX-3-Ni were determined at 298 K and 1.01 bar (Table 1). Remarkably, SIFSIX-1-Cu exhibited superb adsorption capacity (11.01 mmol g^{−1}) among SIFSIX materials, while SIFSIX-2-Cu-i and SIFSIX-2-Cu uptake 6.90 and 6.50 mmol g^{−1}, respectively (Table 1). To the best of our knowledge, this extraordinarily high value of 11.01 mmol g^{−1} measured at room temperature and ambient pressure is the highest of all the materials reported under the same condition so far, including top-performing ones such as M(bdc)(ted)_{0.5} (9.97 mmol g^{−1}),^[36] NOTT-300 (Al) (7.1 mmol g^{−1}),^[34] MFM-300(In) (8.28 mmol g^{−1}),^[35] and MFM-202a (10.2 mmol g^{−1}).^[33]

The adsorption isotherms of SO₂ at 298 and 273 K on SIFSIX materials were measured to systematically demonstrate the SO₂ capture ability of these materials at low pressures (Figure 1 and Table 1), as needed by the actual desulfurization process due to the low SO₂ concentration in feed gas. Notably, the measurements were performed using SO₂/N₂ mixed gas with varying SO₂ molar fractions under flow mode.

As can be noted from Figure 1A, the adsorption isotherms of SO₂ on SIFSIX-1-Cu, SIFSIX-2-Cu-i, SIFSIX-3-Ni, and SIFSIX-3-Zn show a steep increase in the low-pressure range and then reach saturation. At an extremely low SO₂ partial pressure of

Table 1. The adsorption capacities of SO₂ in various porous materials at different partial pressure of SO₂. Summary of the adsorption collected at 298 K. Note: The SO₂ adsorption capacities at 0.002, 0.01, and 0.1 bar were determined using SO₂/N₂ mixed gas with varying SO₂ molar fractions under flow mode, while the SO₂ adsorption capacities at 1.0 bar were determined using SO₂ pure gas.

Materials	SO ₂ uptake [mmol g ^{−1}]				Selectivity for SO ₂ /CO ₂ at 10/90 mixture	Selectivity for SO ₂ /N ₂ at 10/90 mixture	Selectivity for SO ₂ /CH ₄ at 10/90 mixture	Q _{st} [SO ₂ kJ mol ^{−1}]
	0.002 bar ^{a)}	0.01 bar ^{a)}	0.1 bar ^{a)}	1.0 bar				
SIFSIX-1-Cu	1.80	3.43	8.74	11.01	70.7	3145.7	1241.4	36.1
SIFSIX-2-Cu-i	2.31	4.16	6.01	6.90	87.1	3103.2	1017.1	38.1
SIFSIX-3-Zn	0.98	1.68	1.89	2.10	—	506.7	276.0	45.2
SIFSIX-3-Ni	1.39	2.43	2.55	2.74	—	701.8	371.6	43.2
SIFSIX-2-Cu	—	—	—	6.50	—	—	—	—
Ni(bdc)(ted) _{0.5} ^[36]	—	—	3.50	9.97	—	—	—	—
Zn-MOF-74 ^[30]	—	3.03 ^{b)}	—	—	—	—	—	—
MFM-300(In) ^[35]	—	—	—	8.28	50 ^{d)}	2700 ^{d)}	—	34.5/39.6 ^{c)}
MFM-202a ^[33]	—	—	3.0	10.2	—	—	—	35
NOTT-300 (Al) ^[34]	—	—	—	7.1 ^{f)}	—	—	—	—
P(TMGA-co-MBA) ^[40]	—	—	—	4.06	—	—	—	—
Activated Carbon ^[41]	—	—	—	3.3 ^{c)}	—	—	—	—

^{a)}Partial pressure of SO₂; ^{b)}Dynamic adsorption capacity; ^{c)}At the temperature of 323 K and pressure of 0.46 bar; ^{d)}These data were read from the figures of ref. [35]; ^{e)}Highest Q_{st} values at different surface coverage; ^{f)}At the temperature of 298 K.

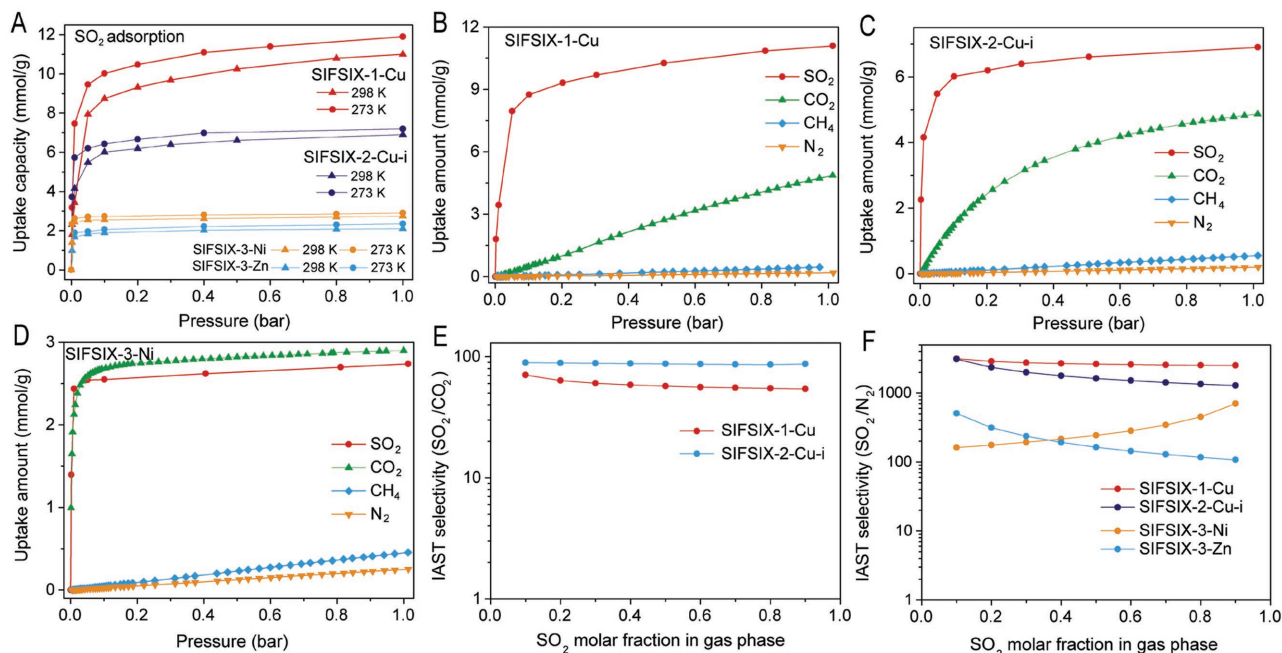


Figure 1. A) SO_2 adsorption isotherms of SIFSIX-1-Cu, SIFSIX-2-Cu-i, SIFSIX-3-Zn, and SIFSIX-3-Ni at 273 and 298 K. Adsorption isotherms for SO_2 , CO_2 , CH_4 and N_2 on B) SIFSIX-1-Cu, C) SIFSIX-2-Cu-i, and D) SIFSIX-3-Ni at 298 K. Note: SO_2 isotherms were measured using SO_2/N_2 mixed gas with varying SO_2 molar fractions under flow mode. CO_2 , CH_4 , and N_2 isotherms were measured using single-component gas. IAST selectivities of SIFSIX materials with E) SO_2/CO_2 mixtures and F) SO_2/N_2 mixtures with varying SO_2 molar fractions in gas phase at 100 kPa.

0.002 bar (2000 ppm) and 298 K, SIFSIX-2-Cu-i rapidly uptake as high as $2.31 \text{ mmol g}^{-1} \text{ SO}_2$ (Figure 1C and Table 1), exceeding the capacity of SIFSIX-1-Cu (1.80 mmol g^{-1}), SIFSIX-3-Zn (0.98 mmol g^{-1}), and SIFSIX-3-Ni (1.39 mmol g^{-1}) (Figure 1B,D and Table 1). This excellent capacity of SO_2 at such a low pressure indicates that SIFSIX-2-Cu-i has great potential in FGD applications. At 298 K, when the partial pressure of SO_2 increased to 0.01 bar, the SO_2 uptake of SIFSIX-2-Cu-i rose to $4.16 \text{ mmol g}^{-1} \text{ SO}_2$, not only still higher than the other three SIFSIX materials but also exceeding the benchmark uptake of Zn-MOF-74 (3.03 mmol g^{-1}). As the pressure of SO_2 further increased to 0.1 bar, the uptake amount of SO_2 at 298 K on SIFSIX-1-Cu increased more rapidly and became more than that on SIFSIX-2-Cu-i, approaching a value of 8.74 mmol g^{-1} while SIFSIX-2-Cu-i exhibits 6.01 mmol g^{-1} , both higher than that ever reported under the same conditions (3.5 mmol g^{-1} by $\text{Ni}(\text{bdc})(\text{ted})_{0.5}$). When the temperature decreased to 273 K, a steep increase in the low-pressure range of isotherms to a high SO_2 capacity was still observed on all these five SIFSIX materials. As shown in Figure 1A, at 273 K and the low SO_2 partial pressure of 0.002 bar, SIFSIX-2-Cu-i exhibited remarkable higher uptake of SO_2 (3.72 mmol g^{-1}), exceeding SIFSIX-1-Cu (3.18 mmol g^{-1}) and SIFSIX-3-Ni (2.34 mmol g^{-1}). With the increase of SO_2 partial pressure, SIFSIX-1-Cu exhibited higher uptake than SIFSIX-2-Cu-i, SIFSIX-3-Ni, and SIFSIX-3-Zn within the whole range of 0.01–1.01 bar. Overall, the results in Table 1 and Figure 1A demonstrate that exceptional SO_2 capacity can be afforded by SIFSIX materials from atmospheric to very low pressures, even more superior at low pressures.

To evaluate the selectivity of SO_2 to other typical gases in gas desulfurization processes, adsorption isotherms of CO_2 , CH_4 ,

and N_2 on SIFSIX materials were collected at 298 K using pure gas. Although both CO_2 and SO_2 are acidic gases, the CO_2 isotherms on SIFSIX-1-Cu show dramatically different adsorption behaviors than SO_2 adsorption isotherms (Figure 1B,C). These dramatic differences between SO_2 and CO_2 adsorption behavior and capacity, especially at low pressures, offer a great potential of selective recognition of SO_2 toward CO_2 on SIFSIX-1-Cu and SIFSIX-2-Cu-i. In addition, SIFSIX-1-Cu and SIFSIX-2-Cu-i only adsorbed 0.45 and $0.55 \text{ mmol g}^{-1} \text{ CH}_4$ at 298 K and 1.0 bar (Figure 1A,B), respectively, which are negligible compared to SO_2 uptake capacity. Furthermore, the uptake amount of N_2 was much lower than CH_4 (Figure 1B–D). As for the case of SIFSIX-3-Ni (Figure 1D) and SIFSIX-3-Zn (Figure S4, supporting information), the CO_2 capacity was higher than the SO_2 capacity, and CH_4 and N_2 were still rarely adsorbed.

In order to further address the separation capability of SIFSIX materials in different gas desulfurization processes, SO_2/CO_2 and SO_2/N_2 separation selectivity were determined using ideal adsorbed solution theory (IAST) calculations as a function of varying SO_2 composition (from 0.1 to 0.9).^[42,43] Notably, in these IAST calculations, the SO_2 isotherms on SIFSIX materials were measured using SO_2/N_2 mixed gas, which might slightly underestimate the selectivity. As shown in Figure 1E, SIFSIX-1-Cu shows excellent SO_2/CO_2 separation selectivity (54–70) over a wide range of SO_2 molar fraction in gas phase (0.1–0.9), especially in the low concentration range. Even better, SIFSIX-2-Cu-i exhibits record SO_2/CO_2 selectivity (86–89) within 0.1–0.9 molar fraction of SO_2 . Considering the fact of low SO_2 concentration in typical flue gas ($\text{SO}_2/\text{CO}_2/\text{N}_2$), this large SO_2/CO_2 selectivity endows SIFSIX-1-Cu and SIFSIX-2-Cu-i with potential in FGD process. This is crucial to realize

a thorough removal of trace SO₂ from flue gas before the CO₂ scrubbing process to ensure the activity of CO₂ adsorbent. To the best of our knowledge, the SO₂/CO₂ IAST selectivity on SIFSIX-2-Cu-i (86–89) and SIFSIX-1-Cu (54–70) sets new benchmarks for SO₂/CO₂ separation. The separation selectivities of SO₂/N₂ and SO₂/CH₄ on the SIFSIX materials were as well estimated by IAST. Figure 1 F shows the high SO₂/N₂ selectivities on SIFSIX-1-Cu (2510–3145) and SIFSIX-2-Cu-i (1285–3103) over a wide range of SO₂ molar fraction in gas phase (0.1–0.9). Moreover, high SO₂/CH₄ selectivities (Figure S5, Supporting Information) over the same range of SO₂ molar fraction were also achieved on SIFSIX-1-Cu (992–1241), SIFSIX-2-Cu-i (422–1017), and SIFSIX-3-Ni (86–371). Therefore, SIFSIX-1-Cu and SIFSIX-2-Cu-i fulfill the requirements by FGD technology, natural-gas purification and other SO₂-separation processes for both SO₂ capacity and selectivity.

To unravel the nature of the interactions between SO₂ molecule and SIFSIX materials, we performed modeling studies using first-principles DFT-D (dispersion-corrected density functional theory) calculations. When trapped within the pore of SIFSIX-1-Cu, SO₂ gets adsorbed primarily through the S^{δ+}...F^{δ-} electrostatic interaction (Figure 2) with SiF₆⁻ anion and the multiple O^{δ-}...H^{δ+} dipole–dipole interactions with the 4,4'-bipyridine linker (Figure 2B). The DFT-D calculated S...F distance is ≈2.6 Å (Figure 2A), much smaller than the sum of the van der Waals radii of S and F (3.3 Å), indicating the considerable strength of this interaction that arises from the negative nature of SiF₆²⁻ ion and positive charge of S atom. Simultaneously, the two oxygen atoms of SO₂ molecule are bonded by the 4,4'-bipyridine linker through multiple dipole–dipole interactions, especially the O^{δ-}...H^{δ+} interactions between oxygen atoms and aromatic hydrogens with a distance of 2.39–3.30 Å (Figure 2B). These multiple synergistic interactions enable the specific recognition of SO₂ molecules through grasping every atoms of the adsorbed SO₂, with a calculated strong adsorption energy (ΔE) of 50.3 kJ mol⁻¹. Thanks to the four equivalent F sites and four equivalent aromatic linkers, four SO₂ molecules were trapped firmly by the host–guest S^{δ+}...F^{δ-} and O^{δ-}...H^{δ+} interactions per unit cell. After that, it is noticed that there are still occupiable pore space in the unit

cell of SIFSIX-1-Cu (between the F sites, along crystallography *c* direction) to accommodate more SO₂ guests. DFT-D calculations showed that two more SO₂ molecules could be trapped in this space as the secondary adsorption, through the dipole–dipole interactions with the channel pore surface and the intermolecular interaction (mainly dipole–dipole interaction) with the SO₂ adsorbed at the primary sites. The ΔE of SO₂ on this site was 38.7 kJ mol⁻¹, with a calculated nearest S_{site2}...O_{site1} distance of 3.6 Å. As a result, six SO₂ were trapped within per unit cell of SIFSIX-1-Cu, four of which were primarily adsorbed via host–guest interactions and the other two were secondarily accommodated mainly via guest–guest interaction with the primary SO₂.

Previous studies have shown that the intermolecular distance in SO₂ liquid tested from X-ray diffraction and neutron studies were centered at 3.5, 4.5, and 5.6 Å with different types of orientations.^[44,45] As clearly shown in Figure 2A, the intermolecular distance of adsorbed SO₂(I) and SO₂(II) is 3.32, 3.56, and 4.07 Å, respectively, within the distance range of the liquid SO₂. These abovementioned data visualize the dense packing of “SO₂ clusters” within the confined electrostatic nanospace of SIFSIX-1-Cu, in consequence of the synergistic host–guest and guest–guest interactions. It is worth noting that this dense packing of “SO₂ clusters” at ambient temperature and low pressure has rarely been reported in common porous adsorbents.

The dense packing of SO₂ clusters within SIFSIX materials is not only the result of the unique pore chemistry but also the optimal pore size. When the organic linker in SIFSIX-1-Cu was replaced by a longer analog, 4,4'-dipyridylacetylene, the resulted SIFSIX-2-Cu showed a weaker interaction with SO₂ (44.2 kJ mol⁻¹) than SIFSIX-1-Cu. The S...F electrostatic interaction was basically of the same nature and strength in the two isoreticular MOFs, implied by the very similar S...F distances, but the dipole–dipole interaction between SO₂ and the 4,4'-dipyridylacetylene linker was slightly weaker than the 4,4'-bipyridine case because of the larger channel pore size of this SIFSIX material. The experimental SO₂ capacity of SIFSIX-2-Cu at room temperature and 1 bar was 6.5 mmol g⁻¹, equivalent to ≈3.7 SO₂ per unit cell. This is lower than the capacity of SIFSIX-1-Cu that was 11.0 mmol g⁻¹ and equivalent to

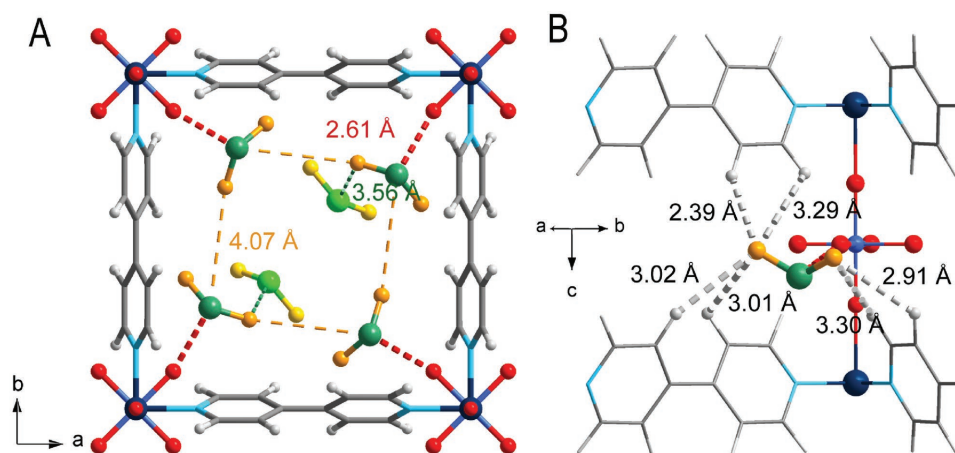


Figure 2. A,B) DFT-D calculated SO₂ adsorption binding sites in SIFSIX-1-Cu viewing in two different directions. Color code: F, red; Si, light blue; C, gray; H, light gray; N, sky blue; Cu, dark teal; O, orange; S, sea green (Note: the secondary adsorbed SO₂ molecules were highlighted with bright color).

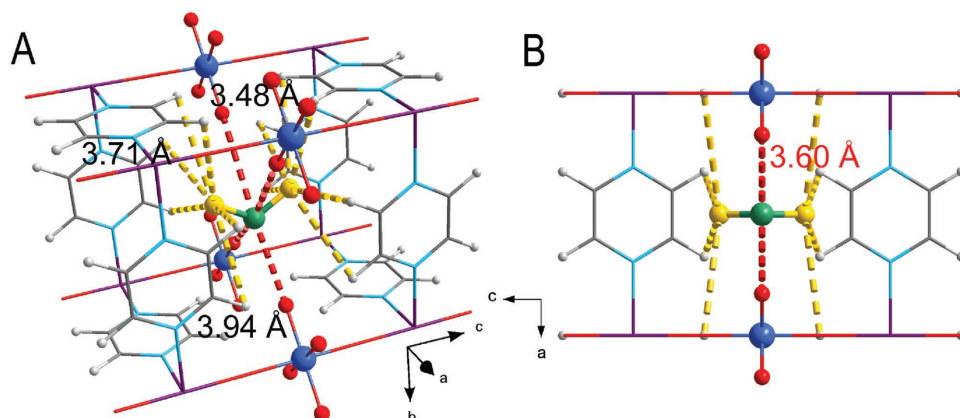


Figure 3. A,B) DFT-D calculated SO_2 adsorption binding sites in SIFSIX-3-Zn viewing in two different directions. Color code: F, red; Si, light blue; C, gray; H, light gray; N, sky blue; Zn, violet; O, orange; S, sea green.

≈ 5.7 SO_2 per unit cell. A too small pore size also goes against the uptake of SO_2 . In SIFSIX-3-Zn, the channel pore size is small due to the much shorter linker pyrazine. DFT-D calculations show that SO_2 molecules get preferentially adsorbed at the center of the 1D channel of SIFSIX-3-Zn along the crystallography c -axis. Although the calculated ΔE of SO_2 with SIFSIX-3-Zn was 54.1 kJ mol^{-1} , slightly higher than that in SIFSIX-1-Cu, the much smaller pore volume captured less SO_2 than SIFSIX-1-Cu. The much longer $\text{S} \cdots \text{F}$ distance (3.60 \AA) demonstrates a weaker $\text{S}^{\delta+} \cdots \text{F}^{\delta-}$ interaction between SO_2 and SIFSIX-3-Zn (Figure 3) than the SIFSIX-1-Cu case, and the grasp of one SO_2 in SIFSIX-3-Zn consumes four times as much F sites as in SIFSIX-1-Cu.

The significance of a well-designed pore chemistry and pore size on the dense packing of SO_2 clusters was further highlighted by the modeling on SIFSIX-2-Cu-i. Although the organic linker in SIFSIX-2-Cu-i is the same as that in SIFSIX-2-Cu, the framework interpenetration in SIFSIX-2-Cu-i enables the size of its unit cell approximately half of that of SIFSIX-2-Cu with a more compact SiF_6^{2-} distribution (Figure 4). DFT-D calculation showed that the $\text{S} \cdots \text{F}$ distance in this MOF is $\approx 2.44 \text{ \AA}$, lower than those in other modeled SIFSIX materials, indicating a strong $\text{S}^{\delta+} \cdots \text{F}^{\delta-}$ electrostatic interaction between SO_2 and SiF_6^{2-} . On the other hand, the two O atoms of SO_2 interact with the H atoms of 4,4'-dipyridylacetylene through multiple

$\text{O}^{\delta-} \cdots \text{H}^{\delta+}$ interactions, with $\text{O} \cdots \text{H}$ distances of $2.79\text{--}3.34 \text{ \AA}$ (Figure 4A). In consequence, every atom of the adsorbed SO_2 was grasped by the pore surface of SIFSIX-2-Cu-i through these multiple synergistic host-guest interactions, with a ΔE of $\approx 50.2 \text{ kJ mol}^{-1}$. This is comparable to that in SIFSIX-1-Cu ($\approx 50.3 \text{ kJ mol}^{-1}$). The two SiF_6^{2-} anions on the diagonal of each unit cell in SIFSIX-2-Cu-i enables the adsorption of two SO_2 by the host-guest $\text{S}^{\delta+} \cdots \text{F}^{\delta-}$ and $\text{O}^{\delta-} \cdots \text{H}^{\delta+}$ interactions. Interestingly, because those two SO_2 molecules are located very close to each other, with the nearest $\text{S} \cdots \text{O}$ distance of only $\approx 3.2 \text{ \AA}$, which enhance the guest-guest interactions (Figure 4A,B). The cooperation of the host-guest and guest-guest interactions affords the formation of SO_2 clusters within the confined electrostatic nanospace of SIFSIX-2-Cu-i. The nearest $\text{S} \cdots \text{O}$ distance of $\approx 3.2 \text{ \AA}$ between two neighboring adsorbed SO_2 is comparable to the intermolecular distance ($3.5\text{--}5.6 \text{ \AA}$) in liquid crystal SO_2 phase and even slightly smaller than that in SIFSIX-1-Cu, implying a dense packing of SO_2 clusters within the pores of SIFSIX-2-Cu-i that enables the excellent uptake of SO_2 at low partial pressures. As presented in Table 1, the experimental SO_2 adsorption capacity of SIFSIX-2-Cu-i at room temperature and 0.01 bar was as large as 4.16 mmol g^{-1} , much higher than those in SIFSIX-1-Cu (3.43 mmol g^{-1}), SIFSIX-3-Zn and SIFSIX-3-Ni. Even if at 0.002 bar (2000 ppm) the SO_2 capacity was as high as 2.26 mmol g^{-1} . Overall, DFT-D calculations on the different

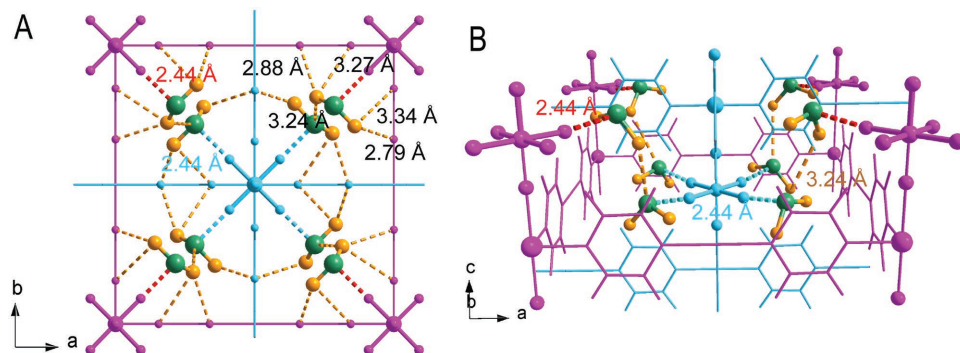


Figure 4. A,B) DFT-D calculated SO_2 adsorption sites in SIFSIX-2-Cu-i viewing in two different directions, and C) crystal structure obtained from Rietveld refinement of PXRD data on SO_2 -loaded SIFSIX-2-Cu-i. (Note: the different nets are highlighted in magenta and cyan for clarity).

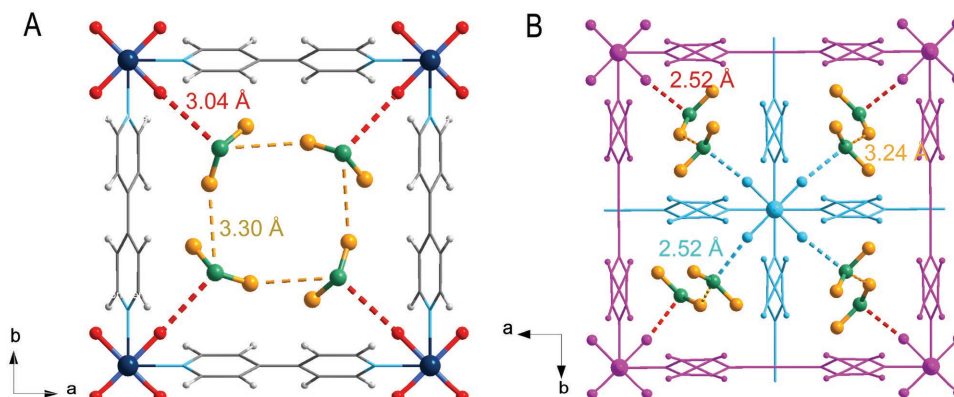


Figure 5. A,B) Crystal structure obtained from Rietveld refinement of PXRD data on SO₂-loaded SIFSIX-1-Cu (A) and SIFSIX-2-Cu-i (B).

SIFSIX materials manifest that the excellent SO₂ capture performance of SIFSIX-1-Cu and SIFSIX-2-Cu-i can be attributed to the synergetic host–guest binding (electrostatic and dipole–dipole interactions) and cooperative guest–guest interactions within the confined electrostatic nanospace of moderate size to form SO₂ clusters.

To provide experimental proof for the DFT-D analysis of SO₂–SIFSIX interactions, we have performed Rietveld refinement of the powder X-ray diffraction patterns of SO₂-loaded samples to locate the adsorbed positions of SO₂ molecules in the crystal structure of SIFSIX materials, and the experimental results are well consistent with the DFT-D calculation results. The Rietveld refined data reveals that in the interpenetrated structure of SIFSIX-2-Cu-i, each SO₂ molecule indeed interacts with SIFSIX-2-Cu-i through S^{δ+}...F^{δ-} bonding (2.52 Å) and multiple O^{δ-}...H^{δ+} interactions (Figure 5B). The nearest S...O distance between adjacent SO₂ molecules are 3.2 Å. In SIFSIX-1-Cu, SO₂ also gets adsorbed primarily through the S^{δ+}...F^{δ-} electrostatic interaction with SiF₆⁻ anion (Figure 5A). The S^{δ+}...F^{δ-} distance is 3.04 Å, longer than the modeling results (2.61 Å). Cooperative interactions between adjacent SO₂ molecules are also observed in the crystal structure of SIFSIX-1-Cu•SO₂ with a S...O distance of 3.3 Å.

We also have performed the detailed DFT-D calculations for CO₂/N₂ molecules to illustrate the difference on interactions between SO₂ and N₂/CO₂ molecules. Results show that the calculated C...F distances between CO₂ and SiF₆²⁻ (2.52 and 2.80 Å) in SIFSIX-2-Cu-i (Figure S10, Supporting Information) are longer than those between SO₂ and SiF₆²⁻ binding sites (2.44 Å), indicating that SIFSIX-2-Cu-i interacted more strongly with SO₂ than CO₂. In SIFSIX-1-Cu, the calculated C...F distance for CO₂ (2.60 Å) is comparable to the S...F distance for SO₂ (2.61 Å); however, the calculated O...H distances between CO₂ molecule and 4,4'-bipyridine (2.64–3.58 Å) are longer than that of SO₂ system (2.39–3.30 Å) (Figure S11, Supporting Information). Additionally, the static adsorption energy (Δ*E*) results show that there are much stronger interactions with SO₂ than CO₂ (Δ*E* in SIFSIX-2-Cu-i, 50.2 versus 35.7 kJ mol⁻¹; Δ*E* in SIFSIX-1-Cu, 50.3 vs 31.1 kJ mol⁻¹; Δ*E* in SIFSIX-3-Zn, 54.1 versus 45.7 kJ mol⁻¹).

To confirm the actual SO₂/N₂ and SO₂/CO₂ separation performance on the SIFSIX materials, we conducted experimental breakthrough tests at 298 K and 1.01 bar on SIFSIX-2-Cu-i, SIFSIX-1-Cu, and SIFSIX-3-Ni (Figure 6). SO₂/N₂ mixture

containing 2000 ppm SO₂ was used to mimic the flue gas with low concentration of SO₂. The reason for using SIFSIX-3-Ni rather than SIFSIX-3-Zn is the relatively higher stability of SIFSIX-3-Ni (Figure S15, Supporting Information). As shown in Figure 6A, highly efficient elimination of SO₂ was achieved with clean N₂ eluted from the bed by all the three SIFSIX materials. The breakthrough time of SO₂ on SIFSIX-2-Cu-i (1800 min g⁻¹) exceeded that on SIFSIX-1-Cu and SIFSIX-3-Ni, consistent with the higher SO₂ adsorption capacities of SIFSIX-2-Cu-i (2.31 mmol g⁻¹) than SIFSIX-1-Cu (1.80 mmol g⁻¹) and SIFSIX-3-Ni (1.39 mmol g⁻¹) in static adsorption experiment at 298 K and 0.002 bar (Figure 1A). Additionally, the actual SO₂/CO₂ separation performance on these SIFSIX materials was also confirmed by the breakthrough experiments, in which the SO₂/CO₂ mixture containing 2000 ppm SO₂ was used. As shown in Figure 6B, outstanding efficient separation of SO₂/CO₂ was achieved with clean CO₂ eluted from the bed by SIFSIX-1-Cu and SIFSIX-2-Cu-i, agreeing well with the results of adsorption isotherm and IAST calculations. The superb SO₂/N₂ and SO₂/CO₂ selectivity at very low SO₂ concentrations makes SIFSIX materials very promising for the gas desulfurization applications.

Given that SO₂ is highly corrosive and few porous MOF materials are stable to the presence of SO₂, concerns about material regeneration are raised. Therefore, we conducted cycling breakthrough tests to evaluate the reusability of SIFSIX-2-Cu-i and SIFSIX-1-Cu for SO₂ capture. As the desorption curves shown in the Figure S16 (Supporting Information), SIFSIX materials adsorbed with SO₂ could be fully regenerated by He flow at 313 K. The breakthrough performance of SIFSIX-2-Cu-i and SIFSIX-1-Cu for 0.2/99.8 (SO₂/CO₂) mixture did not declined during 6 and 4 cycles, respectively (Figure 6C,D). And XRD patterns indicated that both of the SIFSIX materials retain their stability after breakthrough experiments (Figure S6, Supporting Information). In addition, moisture (1000 ppm) has slightly effect on the adsorption capacity of SO₂ on SIFSIX-2-Cu-i (Figure S17, Supporting Information) and SIFSIX-2-Cu-i is stable when exposed to humidity (75%) (Figure S18, Supporting Information).

In summary, this work reports the selective recognition and dense packing of the so-called SO₂ clusters in hybrid porous materials with inorganic-anion-pillared metal–organic framework for the first time. The multiple binding sites of anionic and aromatic linkers initiate the specific recognition of SO₂ by host–guest interactions that grasp the every atom of SO₂

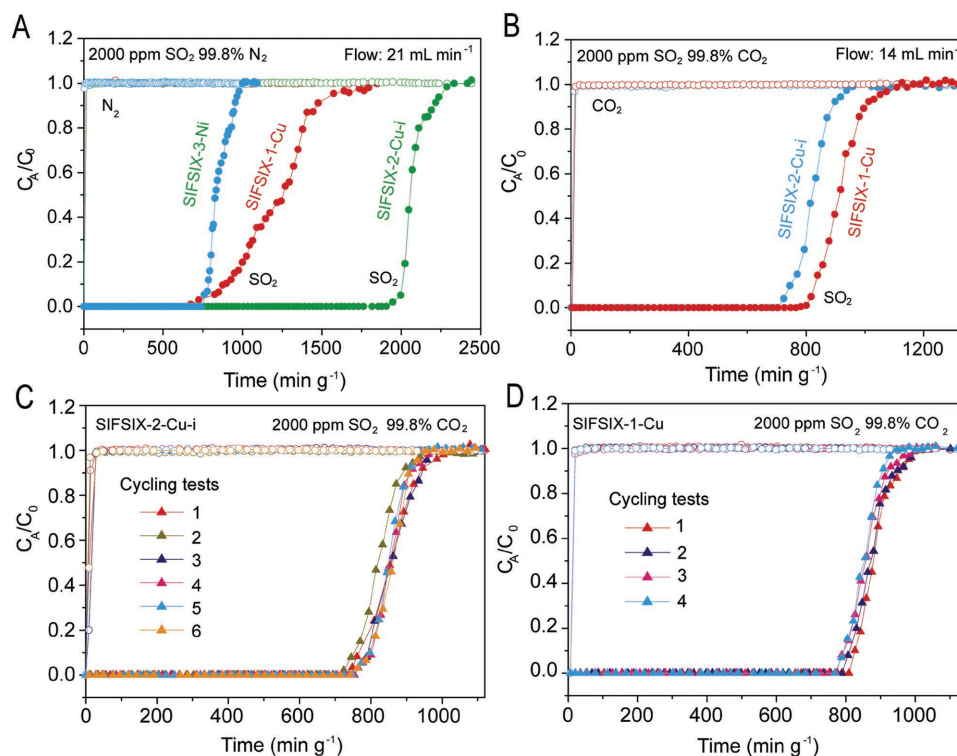


Figure 6. A,B) Experimental column breakthrough curves for SO_2/N_2 (2000 ppm SO_2) separations with SIFSIX-1-Cu, SIFSIX-2-Cu-i, and SIFSIX-3-Ni, and SO_2/CO_2 (2000 ppm SO_2) separations (A) and with SIFSIX-1-Cu and SIFSIX-2-Cu-i (B) at 298 K and 1.01 bar. C,D) Cycling column breakthrough tests for CO_2/SO_2 (2000 ppm SO_2) separations with SIFSIX-2-Cu-i (C) and SIFSIX-1-Cu (D) at 298 K and 1.01 bar (mixed gas flow: 14 mL min⁻¹). In panel (A), open circles are for N_2 , and filled circles are for SO_2 . In panel (B), the open circles are for CO_2 , and the filled circles are for SO_2 . C_A/C_0 , outlet concentration/feed concentration.

firmly, while the dipolar guest–guest interactions between SO_2 molecules enforce the adsorption through promoting the primary binding and enabling secondary adsorption to form SO_2 clusters. A moderate pore size is crucial to afford adequate strength of synergistic host–guest and guest–guest interactions for a dense packing of SO_2 . Thanks to the suitable pore chemistry and size, SIFSIX-1-Cu showed exceptionally high adsorption capacity of SO_2 (11.01 mmol g⁻¹ at 1.01 bar) and selectivity SIFSIX-2-Cu-i exhibited unprecedented SO_2 capacity at low pressures (4.16 mmol g⁻¹ at 0.01 bar and 2.31 mmol g⁻¹ at 0.002 bar) and record SO_2/CO_2 selectivity (86–89), while SIFSIX-1-Cu showed exceptionally high adsorption capacity of SO_2 (11.01 mmol g⁻¹) at 1.01 bar and also excellent SO_2/CO_2 selectivity (54–70). Additionally, extraordinarily high SO_2/N_2 selectivity was also achieved by SIFSIX-2-Cu-i (1285–3103) and SIFSIX-1-Cu (2510–3145). As further confirmed by the breakthrough experiments for mixed gases containing 2000 ppm SO_2 , this excellent performance sets a new benchmark in the highly efficient elimination of SO_2 from flue gas or natural gas even if with a low SO_2 concentration, and this work will be also instructive for the design of porous materials for other gas-purification processes.

Experimental Section

Materials: SIFSIX materials including SIFSIX-1-Cu, SIFSIX-2-Cu, SIFSIX-2-Cu-i, SIFSIX-3-Zn, and SIFSIX-3-Ni were synthesized as

previously described in refs. [19] and [24] (see the Supporting Information for details).^[19,24]

SO_2 Adsorption: SO_2 adsorption isotherms at 298 and 273 K were collected using the apparatus in Figure S1 (Supporting Information). Activated samples were packed in a glass container which was partly immersed in a water bath. The SO_2 adsorption isotherms were determined using SO_2/N_2 mixed gas with varying SO_2 molar fractions under flow mode. Note: the adsorption of SO_2 at 1.01 bar was measured with pure SO_2 at flow mode. At the beginning of this experiment, the activated sample was loaded in the glass container which was full of pure N_2 atmosphere at 760 mmHg. Then, the SO_2/N_2 mixed gas (e.g., 0.002/99.998) was introduced at a constant flow at 760 mmHg. Adsorption equilibrium was reached until the weight of glass container kept constant and did not change. The SO_2 uptake was calculated based on the weight change before and after dynamic adsorption (see the Supporting Information for more detailed adsorption procedures).

Breakthrough Tests: The breakthrough experiments were carried out in a dynamic gas breakthrough equipment (see Figure S2 in the Supporting Information).^[39] All experiments were conducted using a stainless steel column (4.6 mm inner diameter \times 50 mm). According to the different particle size and density of the sample powder, the weight packed in the column was: SIFSIX-1-Cu powder (0.21 g), SIFSIX-2-Cu-i (0.21 g), and SIFSIX-3-Ni (0.50 g), respectively. The column packed with sample was first purged with He flow (15 mL min⁻¹) for 12 h at room temperature (25 °C). The mixed gas of $\text{SO}_2/\text{N}_2 = 0.2/99.8$ (v/v) was then introduced at 21 mL min⁻¹, and $\text{SO}_2/\text{CO}_2 = 0.2/99.8$ (v/v) was introduced at 14 mL min⁻¹. Outlet gas from the column was monitored using gas chromatography (GC-2010 plus) with a thermal conductivity detector (TCD) coupled with a FID. The gas mixture was separated by a capillary column (Agilent GS-GASPRO, $\Phi 0.32 \times 60$ m). The concentration of SO_2 , CO_2 or N_2 in the outlet gas was monitored by the TCD. After the

breakthrough experiment, the sample was regenerated with He flow (7 to 15 mL min⁻¹) for 6–20 h.

Density-Functional Theory Calculations: First-principles density-functional theory (DFT) calculations were performed using the Quantum-Espresso package. A semi-empirical addition of dispersive forces to conventional DFT was included in the calculation to account for van der Waals interactions.^[46] Vanderbilt-type ultrasoft pseudopotentials and generalized gradient approximation with Perdew–Burke–Ernzerhof exchange correlation were used. A cutoff energy of 544 eV and a $2 \times 2 \times 4$ k-point mesh (generated using the Monkhorst–Pack scheme) were found to be enough for the total energy to converge within 0.01 meV atom⁻¹. The structure of SIFSIX MOFs was first optimized. The optimized structures are good matches for the experimentally determined crystal structures of the coordination networks. Various guest gas molecules were then introduced to various locations of the channel pore, followed by a full structural relaxation. To obtain the gas binding energy, an isolated gas molecule placed in a supercell (with the same cell dimensions as the MOF crystal) was also relaxed as a reference. The static binding energy (at $T = 0$ K) was then calculated using: $E_B = E(\text{MOF}) + E(\text{gas}) - E(\text{MOF} + \text{gas})$.

Fitting of Isotherms: The isotherm data for SO₂, CO₂, CH₄, and N₂ in SIFSIX-1-Cu, SIFSIX-2-Cu-i, SIFSIX-3-Zn, and SIFSIX-3-Ni were fitted with either the Langmuir–Freundlich isotherm model:

$$q = q_{\text{sat}} \frac{bp^v}{1 + bp^v} \quad (1)$$

with T -dependent parameters b :

$$b = b_0 \exp\left(\frac{E}{RT}\right) \quad (2)$$

IAST Calculations of Adsorption Selectivities: The adsorption selectivity for C₂H₂/C₂H₄ separation is defined by:

$$S_{\text{ads}} = \frac{q_1/q_2}{p_1/p_2} \quad (3)$$

where q_1 and q_2 are the molar loadings in the adsorbed phase in equilibrium with the bulk gas phase with partial pressures p_1 and p_2 .

Supporting Information

Supporting Information is available from the Wiley Online Library or from the author.

Acknowledgements

This work was supported by the National Natural Science Foundation of China (Grant No. 21436010), National Program for Support of Top-Notch Young Professionals (to H. X.), National Key Research and Development Plan (Grant No. 2016YFB0301500), Zhejiang Provincial Natural Science Foundation of China (Grant No. LR13B060001), and the Welch Foundation (Grant No. AX-1730). The structures of SIFSIX-1-Cu-SO₂ (reference numbers CCDC 1545669) and SIFSIX-2-Cu-i-SO₂ (CCDC 1545670) are available free of charge from the Cambridge Crystallographic Data Centre via www.ccdc.cam.ac.uk/data_request/cif.

Conflict of Interest

The authors declare no conflict of interest.

Keywords

adsorption, gas purification, ionic hybrid porous materials, SO₂ cluster, sulfur dioxide

Received: December 22, 2016

Revised: April 25, 2017

Published online: May 31, 2017

- [1] A. Laurent, N. Espinosa, *Energy Environ. Sci.* **2015**, *8*, 689.
- [2] M. W. Ryberg, M. Owsianiak, A. Laurent, M. Z. Hauschild, *Energy Environ. Sci.* **2015**, *8*, 2435.
- [3] Z. Klimont, S. J. Smith, J. Cofala, *Environ. Res. Lett.* **2013**, *8*, 014003.
- [4] Y. Wang, Q. Q. Zhang, K. He, Q. Zhang, L. Chai, *Atmos. Chem. Phys.* **2013**, *13*, 2635.
- [5] Y. Zhao, L. Duan, J. Xing, T. Larssen, C. P. Nielsen, J. M. Hao, *Environ. Sci. Technol.* **2009**, *43*, 8021.
- [6] Y. Xu, R. H. Williams, R. H. Socolow, *Energy Environ. Sci.* **2009**, *2*, 459.
- [7] R. Pacciani, J. Torres, P. Solsona, C. Coe, R. Quinn, J. Hufton, T. Golden, L. F. Vega, *Environ. Sci. Technol.* **2011**, *45*, 7083.
- [8] R. K. Srivastava, W. Jozewicz, C. Singer, *Environ. Prog.* **2001**, *20*, 219.
- [9] S. Ding, F. Liu, X. Y. Shi, K. Liu, Z. H. Lian, L. J. Xie, H. He, *ACS Appl. Mater. Interfaces* **2015**, *7*, 9497.
- [10] J. S. Valente, R. Quintana-Solorzano, *Energy Environ. Sci.* **2011**, *4*, 4096.
- [11] K. Chen, W. Lin, X. Yu, X. Luo, F. Ding, X. He, H. Li, *AIChE J.* **2015**, *61*, 2028.
- [12] P. Córdoba, *Fuel* **2015**, *144*, 274.
- [13] X. Wang, X. Ma, S. Zhao, B. Wang, C. Song, *Energy Environ. Sci.* **2009**, *2*, 878.
- [14] R. Tailor, M. Abboud, A. Sayari, *Environ. Sci. Technol.* **2014**, *48*, 2025.
- [15] K.-J. Chen, H. S. Scott, D. G. Madden, T. Pham, A. Kumar, A. Bajpai, M. Lusi, K. A. Forrest, B. Space, J. J. Perry IV, M. J. Zaworotko, *Chem* **2016**, *1*, 753.
- [16] P.-Q. Liao, W.-X. Zhang, J.-P. Zhang, X.-M. Chen, *Nat. Commun.* **2015**, *6*, 8697.
- [17] H.-C. Zhou, J. R. Long, O. M. Yaghi, *Chem. Rev.* **2012**, *112*, 673.
- [18] J.-R. Li, J. Sculley, H.-C. Zhou, *Chem. Rev.* **2012**, *112*, 869.
- [19] P. Nugent, Y. Belmabkhout, S. D. Burd, A. J. Cairns, R. Luebke, K. Forrest, T. Pham, S. Q. Ma, B. Space, L. Wojtas, M. Eddaoudi, M. J. Zaworotko, *Nature* **2013**, *495*, 80.
- [20] A. Cadiau, K. Adil, P. M. Bhatt, Y. Belmabkhout, M. Eddaoudi, *Science* **2016**, *353*, 137.
- [21] S. Yang, A. J. Ramirez-Cuesta, R. Newby, V. Garcia-Sakai, P. Manuel, S. K. Callear, S. I. Campbell, C. C. Tang, M. Schroder, *Nat. Chem.* **2015**, *7*, 121.
- [22] T.-L. Hu, H. Wang, B. Li, R. Krishna, H. Wu, W. Zhou, Y. Zhao, Y. Han, X. Wang, W. Zhou, Z. Yao, S. Xiang, B. Chen, *Nat. Commun.* **2015**, *6*, 7328.
- [23] E. D. Bloch, W. L. Queen, R. Krishna, J. M. Zadrozny, C. M. Brown, J. R. Long, *Science* **2012**, *335*, 1606.
- [24] S.-I. Noro, R. Kitaura, M. Kondo, S. Kitagawa, T. Ishii, H. Matsuzaka, M. Yamashita, *J. Am. Chem. Soc.* **2002**, *124*, 2569.
- [25] Z. Bao, G. Chang, H. Xing, R. Krishna, Q. Ren, B. Chen, *Energy Environ. Sci.* **2016**, *9*, 3612.
- [26] W.-Y. Gao, W. Yan, R. Cai, K. Williams, A. Salas, L. Wojtas, X. Shi, S. Ma, *Chem. Commun.* **2012**, *48*, 8898.
- [27] Q.-G. Zhai, X. Bu, C. Mao, X. Zhao, P. Feng, *J. Am. Chem. Soc.* **2016**, *138*, 2524.

- [28] O. M. Farha, A. Ö. Yazaydin, I. Eryazici, C. D. Malliakas, B. G. Hauser, M. G. Kanatzidis, S. T. Nguyen, R. Q. Snurr, J. T. Hupp, *Nat. Chem.* **2010**, 2, 944.
- [29] H. Wang, X.-L. Wang, J. Li, *ChemPlusChem* **2016**, 81, 872.
- [30] D. Britt, D. Tranchemontagne, O. M. Yaghi, *Proc. Natl. Acad. Sci. USA* **2008**, 105, 11623.
- [31] T. G. Glover, G. W. Peterson, B. J. Schindler, D. Britt, O. Yaghi, *Chem. Eng. Sci.* **2011**, 66, 163.
- [32] Z. Arcís-Castillo, F. J. Muñoz-Lara, M. C. Muñoz, D. Aravena, A. B. Gaspar, J. F. Sánchez-Royo, E. Ruiz, M. Ohba, R. Matsuda, S. Kitagawa, J. A. Real, *Inorg. Chem.* **2013**, 52, 12777.
- [33] S. Yang, L. Liu, J. Sun, K. M. Thomas, A. J. Davies, M. W. George, A. J. Blake, A. H. Hill, A. N. Fitch, C. C. Tang, M. Schröder, *J. Am. Chem. Soc.* **2013**, 135, 4954.
- [34] S. Yang, J. Sun, A. J. Ramirez-Cuesta, S. K. Callear, W. I. F. David, D. P. Anderson, R. Newby, A. J. Blake, J. E. Parker, C. C. Tang, M. Schröder, *Nat. Chem.* **2012**, 4, 887.
- [35] M. Savage, Y. Cheng, T. L. Easun, J. E. Eyley, S. P. Argent, M. R. Warren, W. Lewis, C. Murray, C. C. Tang, M. D. Frogley, G. Cinque, J. Sun, S. Rudi, R. T. Murden, M. J. Benham, A. N. Fitch, A. J. Blake, A. J. Ramirez-Cuesta, S. Yang, M. Schröder, *Adv. Mater.* **2016**, 28, 8705.
- [36] K. Tan, P. Canepa, Q. Gong, J. Liu, D. H. Johnson, A. Dyevoich, P. K. Thallapally, T. Thonhauser, J. Li, Y. J. Chabal, *Chem. Mater.* **2013**, 25, 4653.
- [37] L. Ding, A. O. Yazaydin, *Phys. Chem. Phys.* **2013**, 15, 11856.
- [38] J. Yu, Y. Ma, P. B. Balbuena, *Langmuir* **2012**, 28, 8064.
- [39] X. Cui, K. Chen, H. Xing, Q. Yang, R. Krishna, Z. Bao, H. Wu, W. Zhou, X. Dong, Y. Han, B. Li, Q. Ren, M. J. Zaworotko, B. Chen, *Science* **2016**, 353, 141.
- [40] L. Wu, D. An, J. Dong, Z. Zhang, B.-G. Li, S. Zhu, *Macromol. Rapid Commun.* **2006**, 27, 1949.
- [41] H. Yi, Z. Wang, H. Liu, X. Tang, D. Ma, S. Zhao, B. Zhang, F. Gao, Y. Zuo, *J. Chem. Eng. Data* **2014**, 59, 1556.
- [42] K. S. Walton, D. S. Sholl, *AIChE J.* **2015**, 61, 2757.
- [43] R. Krishna, *RSC Adv.* **2015**, 5, 52269.
- [44] M. Alvarez, F. J. Bermejo, P. Chieux, E. Enciso, M. Garcia-Hernandez, N. Garcia, J. Alonso, *Mol. Phys.* **1989**, 66, 397.
- [45] B. Post, R. S. Schwartz, I. Fankuchen, *Acta Cryst.* **1952**, 5, 372.
- [46] V. Barone, M. Casarin, D. Forrer, M. Pavone, M. Sambì, A. Vittadini, *Comput. Chem.* **2009**, 30, 934.

ADVANCED MATERIALS

Supporting Information

for *Adv. Mater.*, DOI: 10.1002/adma.201606929

Ultrahigh and Selective SO₂ Uptake in Inorganic Anion-Pillared Hybrid Porous Materials

Xili Cui, Qiwei Yang, Lifeng Yang, Rajamani Krishna, Zhiguo Zhang, Zongbi Bao, Hui Wu, Qilong Ren, Wei Zhou, Banglin Chen,* and Huabin Xing**

Supporting Information

Ultrahigh and Selective SO₂ Uptake in Inorganic Anion-Pillared Hybrid Porous Materials

*Xili Cui, Qiwei Yang, * Lifeng Yang, Rajamani Krishna, Zhiguo Zhang, Zongbi Bao, Hui Wu, Qilong Ren, Wei Zhou, Banglin Chen, * Huabin Xing**

Dr. X. L. Cui, Dr. Q. W. Yang, L. F. Yang, Dr. Z. G. Zhang, Dr. Z. B. Bao, Prof. Q. L. Ren, Prof. H. B. Xing

Key Laboratory of Biomass Chemical Engineering of Ministry of Education, College of Chemical and Biological Engineering, Zhejiang University, Hangzhou 310027, China

E-mail: xinghb@zju.edu.cn yangqw@zju.edu.cn

Prof. R. Krishna

Van' t Hoff Institute for Molecular Sciences, University of Amsterdam, Science Park 904, 1098 XH Amsterdam, Netherlands

Dr. H. Wu, Prof. W. Zhou

Center for Neutron Research, National Institute of Standards and Technology, Gaithersburg, Maryland 20899-6102, USA.

Prof. B. L. Chen

Department of Chemistry, University of Texas at San Antonio, One UTSA Circle, San Antonio, Texas 78249-0698, USA

E-mail: Banglin.Chen@utsa.edu

This PDF file includes:

Materials and Methods

Tables S1-S6

Figures. S3 to S18

Experiments

Materials

Ammonium hexafluorosilicate ((NH)₂SiF₆, 98%, Aldrich), copper (II) tetrafluoroborate hydrate (Cu(BF₄)₂• xH₂O, 98%, Aldrich), zinc hexafluorosilicate hydrate (ZnSiF₆• xH₂O, 99%, Aldrich), 4,4'-bipyridine (C₁₀H₈N₂, 98%, Aldrich), 4-(2-pyridin-4-ylethynyl)pyridine (C₁₂H₈N₂, 98%, Chemsoon), pyrazine (C₄H₄N₂, 99%, Aldrich), methanol (CH₃OH, anhydrous, 99%, Sigma-Aldrich), ethylene glycol (C₂H₆O₂, anhydrous, 99%, Sigma-Aldrich), were purchased and used without further purification.

N₂ (99.999%), CO₂ (99%), CH₄ (99.99%), He (99.999%), SO₂ (99.99%) and mixed gases of (1) SO₂/N₂ = 0.2/99.8 (v/v), (2) SO₂/N₂ = 1/99 (v/v), (3) SO₂/N₂ = 5/95 (v/v), (4) SO₂/N₂ = 10/90 (v/v) were purchased from JinGong Company (China). Mixed gases of (5) SO₂/CO₂ = 0.2/99.8 (v/v) were purchased from Shanghai Wetry Standard Reference Gas Analytical Technology Co. LTD (China).

Synthesis

Synthesis of SIFSIX-1-Cu (Cu(4,4'-bipyridine)₂SiF₆•8H₂O)_n

Firstly, 4,4'-bipyridine (0.35 g) was dissolved in ethylene glycol (40 mL) at 338 K. An aqueous solution (20 mL) of Cu(BF₄)₂•xH₂O (266 mg, 1.12 mmol) and (NH₄)₂SiF₆ (199 mg, 1.12 mmol) was added to the above solution. Then the mixture was heated at 65 °C for 3 h under stirring. The obtained purple powder was filtered, washed with methanol, and was exchanged with methanol for 3 days.^[1]

Synthesis of SIFSIX-2-Cu (Cu(4,4'-bipyridylacetylene)₂SiF₆)_n

An ethanol solution (2.0 mL) of 4,4'-bipyridylacetylene (0.115mmol) was carefully layered onto an ethylene glycol solution (2.0 mL) of CuSiF₆•xH₂O (0.149 mmol). Crystals of SIFSIX-2-Cu were obtained after two weeks. The obtained sample was exchanged with ethanol for 4 days.^[2]

Synthesis of SIFSIX-2-Cu-i (Cu(4,4'-bipyridylacetylene)₂SiF₆).

A methanol solution (4.0 mL) of 4,4'-bipyridylacetylene (0.286 mmol) was mixed with an aqueous solution (4.0 mL) of $\text{Cu}(\text{BF}_4)_2 \cdot x\text{H}_2\text{O}$ (0.26 mmol) and $(\text{NH}_4)_2\text{SiF}_6$ (0.26 mmol) and then heated at 85 °C for 12 h. The obtained sample was exchanged with methanol for 3 days.

[2]

Synthesis of SIFSIX-3-Zn ($\text{Zn}(\text{pyrazine})_2\text{SiF}_6$)_n

A methanol solution (2.0 mL) of pyrazine (1.3 mmol) was carefully layered onto a methanol solution (2.0 mL) of $\text{ZnSiF}_6 \cdot x\text{H}_2\text{O}$ (0.13 mmol). Colourless crystals of SIFSIX-3-Zn were obtained after two days. The obtained sample was exchanged with ethanol for 1 days. [2]

Synthesis of SIFSIX-3-Ni ($\text{Ni}(\text{pyrazine})_2\text{SiF}_6$)_n

A methanol solution (20 mL) of nickel silicofluoride, NiSiF_6 (1 mmol) and pyrazine (2 mmol) was mixed and heated at 85 °C. Blue powder was obtained after 3 days. The obtained sample was exchanged with ethanol for 3 days. [3]

Pure gas adsorption

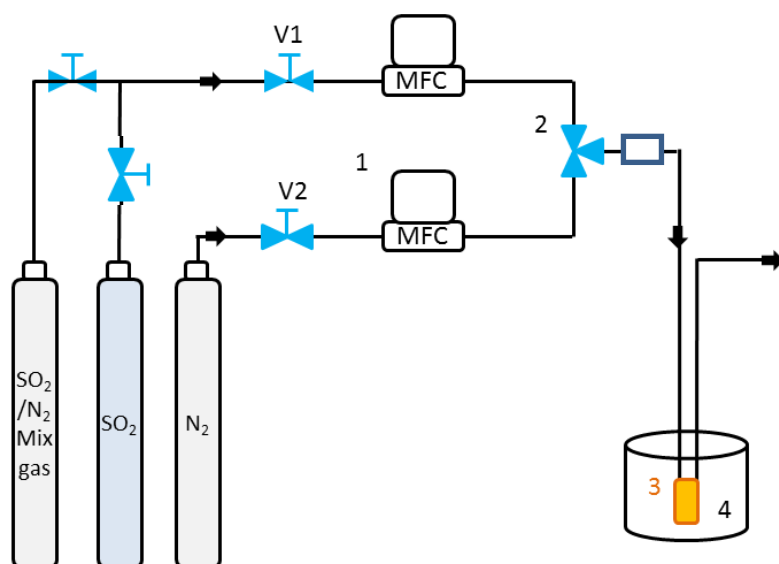
SIFSIX-1-Cu, SIFSIX-2-Cu, SIFSIX-2-Cu-i, and SIFSIX-3-Zn were evacuated at 303 K for 1-2 days until the pressure dropped below 7 μm Hg. SIFSIX-3-Ni was degassed at 105 °C for 15 h under dynamic pressure below 5 μm Hg. N_2 , CO_2 and CH_4 sorption isotherms were collected at 298 K on activated SIFSIX-1-Cu, SIFSIX-2-Cu, SIFSIX-2-Cu-i, SIFSIX-3-Ni and SIFSIX-3-Zn using ASAP 2050 Analyzer (Micromeritics).

SO₂ adsorption

SO_2 adsorption isotherms at 298 K and 273 K were collected using the apparatus in Figure S1. Activated samples were packed in a glass container which was partly immersed in a water bath. The SO_2 adsorption isotherms were determined using SO_2/N_2 mixed gas with varying SO_2 molar fractions under flow mode. Note: the adsorption of SO_2 at 1.0 atm was measured with pure SO_2 at flow mode. At the beginning of this experiment, the activated sample was loaded in the glass container which was full of pure N_2 atmosphere at 760 mmHg. Then the SO_2/N_2 mixed gas (e.g. 0.002/99.998) was introduced at a constant flow at 760 mmHg.

Adsorption equilibrium was reached until the weight of glass container kept constant and didn't change. The SO_2 uptake was calculated based on the weight-change before and after dynamic adsorption. This method will underestimate the SO_2 uptake because the samples were pre-saturated by N_2 but some of N_2 molecules were displaced by the SO_2 molecules. At the adsorption with high SO_2 molar fraction, the weight of unabsorbed SO_2 gases in the glass container was subtracted by blank test.

The detailed adsorption procedures: firstly, SO_2/N_2 (0.002/0.998) mixed gas was introduced into the glass container at a rate of 20 ml min^{-1} . Equilibrium were reached until the weight of glass container kept constant and didn't change. The amount of adsorbed SO_2 at the partial pressure of 0.002 was determined by the electronic balance with $\pm 0.1 \text{ mg}$ accuracy. Then, the uptake capacity of SO_2 at the partial pressure of 0.01, 0.05, 0.1 was measured using SO_2/N_2 (0.01/0.99), SO_2/N_2 (0.05/0.95), SO_2/N_2 (0.1/0.9) mixed gas using the repeated procedures. The higher partial pressure of SO_2 (e.g. 0.4, 0.5, 0.8 1.0) was controlled by changing the flow rate of SO_2 and N_2 .



1. Mass flow controller 2. 3-Way valve 3. Glass container 4. Water bath

Figure S1 Schematic illustration of the apparatus for the SO_2 adsorption experiments.

Breakthrough tests

The breakthrough experiments were carried out in a dynamic gas breakthrough equipment (fig. S2).^[4] All experiments were conducted using a stainless steel column (4.6 mm inner diameter \times 50 mm). According to the different particle size and density of the sample powder, the weight packed in the column was: SIFSIX-1-Cu powder (0.21 g), SIFSIX-2-Cu-i (0.21 g), and SIFSIX-3-Ni (0.50 g), respectively. The column packed with sample was firstly purged with He flow (15 ml min⁻¹) for 12 h at room temperature (25 °C). The mixed gas of SO₂/N₂ = 0.2/99.8 (v/v) was then introduced at 21 ml min⁻¹, and SO₂/CO₂ = 0.2/99.8 (v/v) was introduced at 14 ml min⁻¹. Outlet gas from the column was monitored using gas chromatography (GC-2010 plus) with a thermal conductivity detector (TCD) coupled with a FID. The gas mixture was separated by a capillary column (Agilent GS-GASPRO, Φ 0.32 \times 60 M). The concentration of SO₂, CO₂ or N₂ in the outlet gas was monitored by the TCD. After the breakthrough experiment, the sample was regenerated with He flow (7 to 15 ml min⁻¹) for 6 to 20 hours.

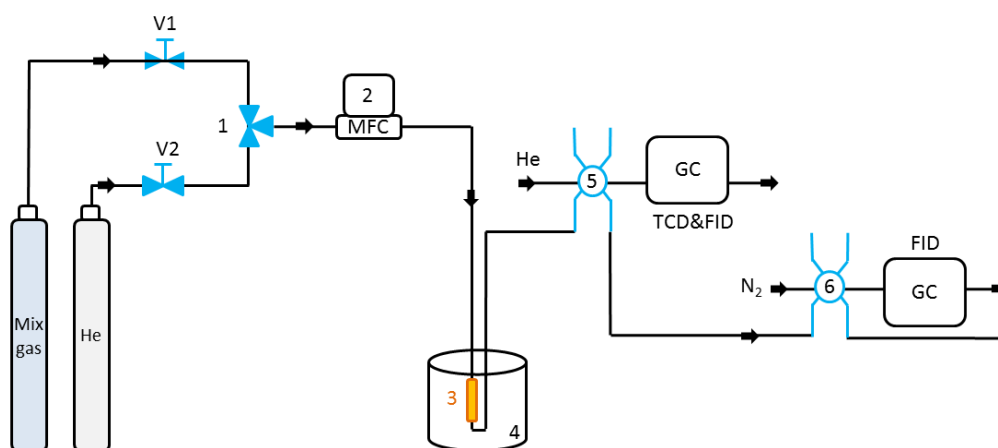


Figure S2 Schematic illustration of the apparatus for the breakthrough experiments.

X-ray diffraction structure analysis

Powder X-ray diffraction patterns were collected using SHIMADZU XRD-6000 diffractometer ($\text{Cu K}\alpha \lambda = 1.540598 \text{ \AA}$) with an operating power of 40 Kv and fixed divergence slit of 0.76 mm. The data were collected in the range of $2\theta = 3\text{-}50^\circ$.

Powder X-ray diffraction patterns of bare and SO_2 -loaded SIFSIX-1-Cu and SIFSIX-2-Cu-i were collected using PANalytical X'Pert Pro diffractometer ($\text{Cu K}\alpha \lambda = 1.540598 \text{ \AA}$) with an operating power of 40 Kv and fixed divergence slit of 0.380 mm. The data were collected in the range of $2\theta = 3\text{-}60^\circ$.

Density-functional theory calculations

First-principles density-functional theory (DFT) calculations were performed using the Quantum-Espresso package. A semi-empirical addition of dispersive forces to conventional DFT was included in the calculation to account for van der Waals interactions.^[5] We used Vanderbilt-type ultrasoft pseudopotentials and generalized gradient approximation (GGA) with Perdew-Burke-Ernzerhof (PBE) exchange correlation. A cutoff energy of 544 eV and a $2\times 2\times 4$ k-point mesh (generated using the Monkhorst-Pack scheme) were found to be enough for the total energy to converge within $0.01 \text{ meV atom}^{-1}$. We first optimized the structure of SIFSIX MOFs. The optimized structures are good matches for the experimentally determined crystal structures of the coordination networks. Various guest gas molecules were then introduced to various locations of the channel pore, followed by a full structural relaxation. To obtain the gas binding energy, an isolated gas molecule placed in a supercell (with the same cell dimensions as the MOF crystal) was also relaxed as a reference. The static binding energy (at $T = 0 \text{ K}$) was then calculated using: $\text{EB} = E(\text{MOF}) + E(\text{gas}) - E(\text{MOF}+\text{gas})$.

Fitting of isotherms

The isotherm data for SO_2 , CO_2 , CH_4 , and N_2 in SIFSIX-1-Cu, SIFSIX-2-Cu-i, SIFSIX-3-Zn, and SIFSIX-3-Ni were fitted with either the Langmuir-Freundlich isotherm model.

$$q = q_{sat} \frac{bp^\nu}{1 + bp^\nu} \quad (1)$$

with T -dependent parameters b

$$b = b_0 \exp\left(\frac{E}{RT}\right) \quad (2)$$

The fitted parameter values are presented in Table S1

Notation

b	Langmuir-Freundlich constant, $\text{Pa}^{-\nu}$
E	energy parameter, J mol^{-1}
p	pressure, Pa
q	component molar loading, mol kg^{-1}
q_{sat}	saturation loading, mol kg^{-1}
R	gas constant, $8.314 \text{ J mol}^{-1} \text{ K}^{-1}$
T	absolute temperature, K

Isosteric heat of adsorption

The binding energy of SO_2 is reflected in the isosteric heat of adsorption, Q_{st} , defined as

$$Q_{\text{st}} = RT^2 \left(\frac{\partial \ln p}{\partial T} \right)_q \quad (3)$$

Figure S3 presents a comparison of the heats of adsorption of SO_2 in various SIFSIX; the calculations are based on the use of the Clausius-Clapeyron equation.

IAST claculations of adsorption selectivities

The adsorption selectivity for $\text{C}_2\text{H}_2/\text{C}_2\text{H}_4$ separation is defined by

$$S_{\text{ads}} = \frac{q_1/q_2}{p_1/p_2} \quad (3)$$

q_1 , and q_2 are the molar loadings in the adsorbed phase in equilibrium with the bulk gas phase with partial pressures p_1 , and p_2 .

Table S1. Langmuir-Freundlich parameter fits for SO₂, CO₂, CH₄, and N₂ in SIFSIX materials. The isotherm data for CH₄, and N₂ were only measured at 298 K, and therefore $E = 0$.

SIFSIX-1-Cu				
	q_{sat} mol kg ⁻¹	b_0 Pa ^{-ν_i}	E kJ mol ⁻¹	ν dimensionless
SO ₂	11.7	9.8×10^{-8}	26	0.72
CO ₂	12	1.12×10^{-13}	33	1.2
CH ₄	12	3.9×10^{-7}	0	1
N ₂	12	1.54×10^{-7}	0	1

SIFSIX-2-Cu-i				
	q_{sat} mol kg ⁻¹	b_0 Pa ^{-ν_i}	E kJ mol ⁻¹	ν dimensionless
SO ₂	7.1	1.33×10^{-6}	23.6	0.62
CO ₂	6.5	4.9×10^{-11}	33	1
CH ₄	12	4.87×10^{-7}	0	1
N ₂	12	1.6×10^{-7}	0	1

SIFSIX-3-Ni				
	q_{sat} mol kg ⁻¹	b_0 Pa ^{-ν_i}	E kJ mol ⁻¹	ν dimensionless
SO ₂	2.7	3.05×10^{-11}	46.2	1.07
CH ₄	12	3.9×10^{-7}	0	1
N ₂	12	2.08×10^{-7}	0	1

SIFSIX-3-Zn				
	q_{sat} mol kg ⁻¹	b_0 Pa ^{-ν_i}	E kJ mol ⁻¹	ν dimensionless
SO ₂	2.25	4.1×10^{-6}	23.5	0.52
CH ₄	12	3.78×10^{-7}	0	1
N ₂	12	2.08×10^{-7}	0	1

Table S2. The volumetric uptake of SO₂ (density per crystal cell volume) in various SIFSIX materials at 1.01 bar.

	Framework density (g cm ⁻³)	C ₂ H ₂ density per crystal cell volume (g cm ⁻³)	
		298 K	283 K 273 K
SIFSIX-1-Cu	0.864	0.609	0.658
SIFSIX-2-Cu-i	1.247	0.551	0.575
SIFSIX-3-Zn	1.574	0.212	0.237
SIFSIX-3-Ni	1.610	0.282	0.299

Table S3. List of atomic positions for SIFSIX-1-Cu·SO₂

Atom	a	b	c
N6	0.00000	0.18296	0.00000
C5	0.00000	0.43393	0.00000
C1	0.03427	0.24303	0.13464
C2	0.03491	0.36849	0.13817
H3	0.06405	0.19281	0.24102
H4	0.06545	0.41511	0.24710
Cu7	0.00000	0.00000	0.00000
Si8	0.00000	0.00000	0.50000
F9	0.00000	0.00000	0.28490
F10	0.10630	0.10630	0.50000
S11	0.28855	0.30438	0.56560
O12	0.40425	0.26932	0.49696
O13	0.21666	0.39012	0.47061

Unit cell parameters	
Formula sum	N C3 H2 Cu Si F2 S0.252 O0.503
Formula weight	197.81 g mol ⁻¹
Space-group	P 422
Cell parameters	a=11.1348 Å b=11.1348 Å c=8.0047 Å α=90.00° β=90.00° γ=90.00°
Cell ratio	a/b=1.0000 b/c=1.3910 c/a=0.7189
Cell volume	992.47 Å ³

Table S4. List of Miller Index of the simulated pattern of SIFSIX-1-Cu•SO₂

2 Theta	h	k	l	d-spacing
7.934	1	0	0	11.1348
11.044	0	0	1	8.00474
11.229	1	1	0	7.87352
13.613	1	0	1	6.49954
15.775	1	1	1	5.61324
15.906	2	0	0	5.56742
17.798	2	1	0	4.97965
19.406	2	0	1	4.57062
20.993	2	1	1	4.22826
22.193	0	0	2	4.00237
22.568	2	2	0	3.93676
22.602	1	0	2	3.76645
23.956	3	0	0	3.71162
24.937	1	1	2	3.56786
25.189	2	2	1	3.53265
25.273	3	1	0	3.52115
26.448	3	0	1	3.36725
27.423	2	0	2	3.24977
27.654	3	1	1	3.2231
28.591	2	1	2	3.11962
28.887	3	2	0	3.08825
31.013	3	2	1	2.88126
31.859	2	2	2	2.80662
32.129	4	0	0	2.78371
32.884	3	0	2	2.7215
33.146	4	1	0	2.7006
33.559	0	0	3	2.66825
33.880	3	1	2	2.64368
34.072	4	0	1	2.62926
34.136	3	3	0	2.62451
34.539	1	0	3	2.59479
35.039	4	1	1	2.55889
35.494	1	1	3	2.52708
35.983	3	3	1	2.49389
36.044	4	2	0	2.48983
36.728	3	2	2	2.44501
37.342	2	0	3	2.40618
37.810	4	2	1	2.37747
38.237	2	1	3	2.35189
39.396	4	0	2	2.28531
40.253	4	1	2	2.23865
40.473	5	0	0	2.22697
40.473	4	3	0	2.22697
40.822	2	2	3	2.20873
41.094	3	3	2	2.19473
41.311	5	1	0	2.18372
41.654	3	0	3	2.16651

42.082	5	0	1	2.14549
42.082	4	3	1	2.14549
42.473	3	1	3	2.12663
42.736	4	2	2	2.11413
42.894	5	1	1	2.10674
43.745	5	2	0	2.06769
44.856	3	2	3	2.01903
42.259	5	2	1	2.00198
45.278	0	0	4	2.00119
46.045	1	0	4	1.96963
46.075	4	4	0	1.96838
46.636	4	3	2	1.94601
46.636	5	0	2	1.94601
46.802	1	1	4	1.93952
47.143	4	0	3	1.92626
47.386	5	1	2	1.91696
47.531	4	4	1	1.91144
47.579	5	3	0	1.90961
47.887	4	1	3	1.89807
48.288	2	0	4	1.88322
48.622	3	3	3	1.87108
49.001	5	3	1	1.85749
49.019	2	1	4	1.85685
49.048	6	0	0	1.85581
49.583	5	2	2	1.83703
49.770	6	1	0	1.83056
50.068	4	2	3	1.82038
50.439	6	0	1	1.80786
51.146	6	1	1	1.78449
51.164	2	2	4	1.78393
51.711	4	4	2	1.76633
51.864	3	0	4	1.76147
51.893	6	2	0	1.76057
52.558	3	1	4	1.73983
52.586	5	4	0	1.73897
53.095	5	3	2	1.72349
53.229	6	2	1	1.71948
53.557	4	3	3	1.70972
53.557	5	0	3	1.70972
53.911	5	4	1	1.69933
54.236	5	1	3	1.68992
54.455	6	0	2	1.68363
54.603	3	2	4	1.67941

Table S5. List of atomic positions for SIFSIX-2-Cu-i•SO₂

Atom	a	b	c
N7	0.00000	0.14897	0.00000
C5	0.00000	0.64726	0.00000
C1	0.02267	0.19911	0.13599
C2	0.02503	0.30009	0.14229
H3	0.03526	0.15749	0.24709
H4	0.03655	0.33606	0.25900
C6	0.00000	0.54419	0.00000
Cu8	0.00000	0.00000	0.00000
Si9	0.00000	0.00000	0.50000
F10	0.00000	0.00000	0.28300
F11	0.08780	0.08780	0.50000
S7	0.19765	0.22777	0.57535
O5	0.26019	0.19711	0.44227
O6	0.12431	0.30126	0.53996

Unit cell parameters	
Formula sum	N C3 H Cu Si F2 S0.17 O0.341
Formula weight	191.591 g mol ⁻¹
Space-group	I 4/ m m m
Cell parameters	a=13.7315 Å c=8.2100 Å
Cell ratio	a/b=1.0000 b/c=1.6725 c/a=0.5979
Cell volume	1548.04 Å ³

Table S6. List of Miller Index of the simulated pattern of SIFSIX-2-Cu-i•SO₂

2 Theta	h	k	l	d-spacing
9.101	1	1	0	9.70963
12.552	1	0	1	7.04657
12.884	2	0	0	6.86575
18.024	2	1	1	4.9175
18.259	2	2	0	4.85482
20.436	3	1	0	4.34228
21.631	0	0	2	4.10502
22.218	3	0	1	3.99784
23.510	1	1	2	3.78099
25.257	2	0	2	3.52329
25.766	3	2	1	3.45482
25.934	4	0	0	3.43287
27.537	3	3	0	3.23654
28.451	2	2	2	3.13464
28.908	4	1	1	3.08613
29.059	4	2	0	3.07046
29.930	3	1	2	2.98304
33.242	5	1	0	2.69297
33.358	1	0	3	2.6839
34.017	4	0	2	2.63341
34.407	4	3	1	2.60445
34.407	5	0	1	2.60445
35.285	3	3	2	2.54159
35.897	2	1	3	2.49969
36.515	4	2	2	2.45875
36.882	5	2	1	2.43513
37.004	4	4	0	2.42741
38.186	5	3	0	2.35493
38.288	3	0	3	2.34886
39.338	6	0	0	2.28858
40.010	5	1	2	2.25169
40.560	3	2	3	2.2224
41.451	6	1	1	2.17666
41.561	6	2	0	2.17114
42.731	4	1	3	2.11439
43.266	4	4	2	2.08944
43.585	5	4	1	2.07488
44.085	0	0	4	2.05251
44.309	5	3	2	2.04268
45.112	1	1	4	2.00813
45.332	6	0	2	1.99892
45.639	6	3	1	1.98617
46.122	2	0	4	1.96652
46.740	7	1	0	1.94193
46.740	5	5	0	1.94193
46.827	4	3	3	1.93852
46.827	5	0	3	1.93852

WILEY-VCH

47.326	6	2	2	1.91923
47.624	7	0	1	1.90794
47.723	6	4	0	1.90422
48.091	2	2	4	1.8905
48.774	5	2	3	1.86558
49.053	3	1	4	1.85565
49.547	7	2	1	1.83828
50.583	7	3	0	1.80303
51.859	4	0	4	1.76164
52.056	7	1	2	1.75542
52.056	5	5	2	1.75542
52.506	6	1	3	1.74143
52.770	3	3	4	1.73335
52.965	6	4	2	1.72741
53.240	6	5	1	1.71916
53.331	8	0	0	1.71644
53.670	4	2	4	1.70637
54.303	5	4	3	1.68798

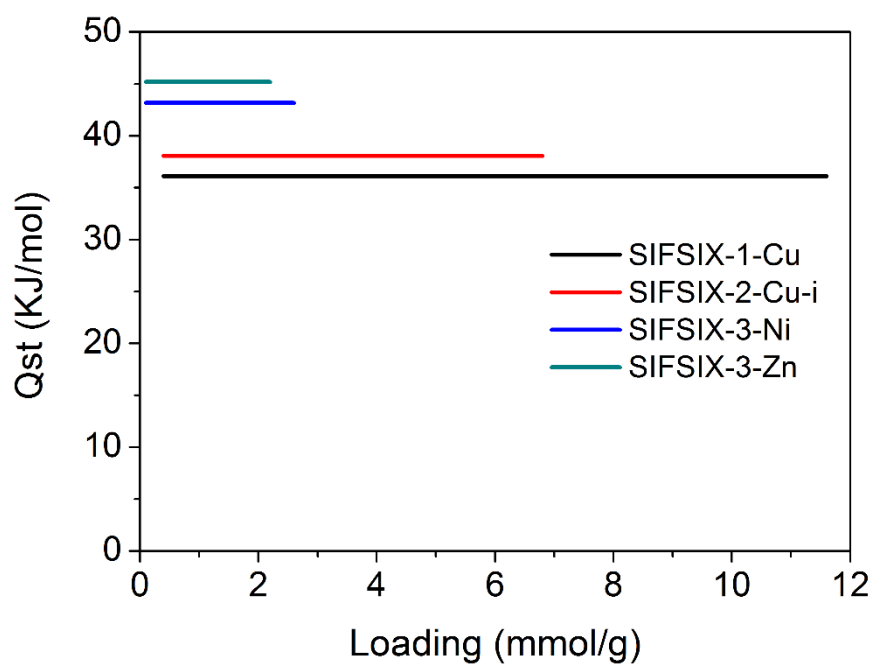


Figure S3 Comparison of Q_{st} of SO_2 adsorption in SIFSIX materials.

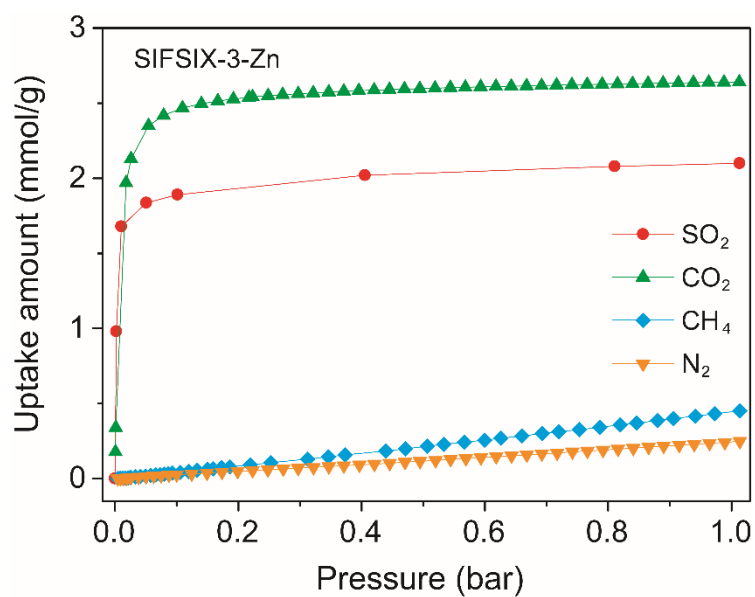


Figure S4 Adsorption isotherms for SO₂, CO₂ and CH₄ on SIFSIX-3-Zn at 298 K and 1.0 bar.

Note: the adsorption isotherm of SO₂ were determined using SO₂/N₂ mixed gas with varying SO₂ molar fractions under flow mode.

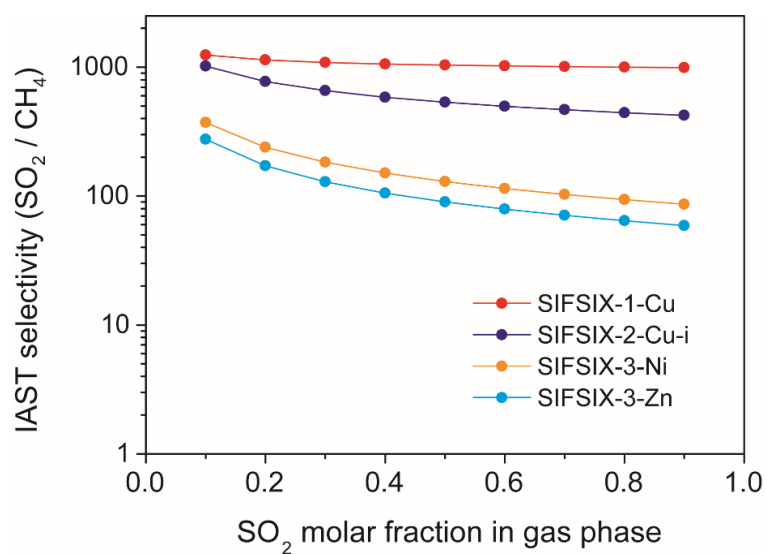


Figure S5 IAST selectivities of SO_2/CH_4 on SIFSIX materials with varying SO_2 molar fractions in gas phase at 100 kPa.

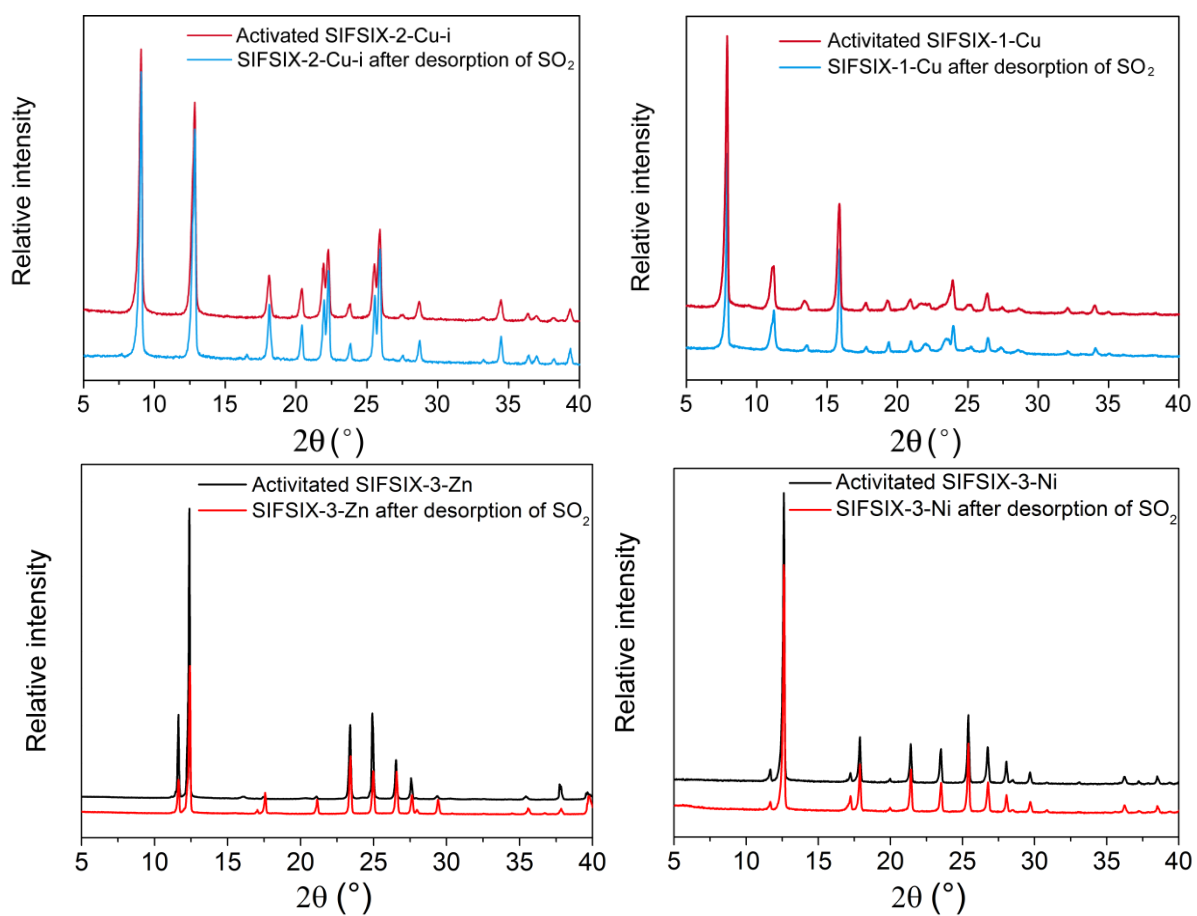


Figure S6. PXRD patterns of sample SIFSIX-2-Cu-i (A), SIFSIX-1-Cu (B), SIFSIX-3-Zn (C) and SIFSIX-3-Ni (D).

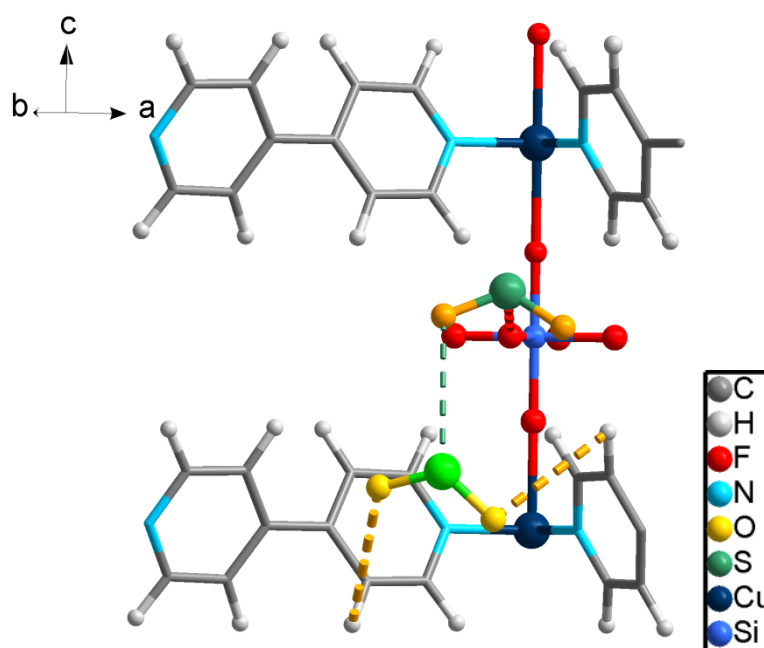


Figure S7 Schematic pictures from DFT-D simulation reveal the SO₂ adsorbed at the secondary adsorption sites of SIFSIX-1-Cu through dipole-dipole interactions. (Note: the secondary adsorbed SO₂ molecules were highlighted with bright colour).

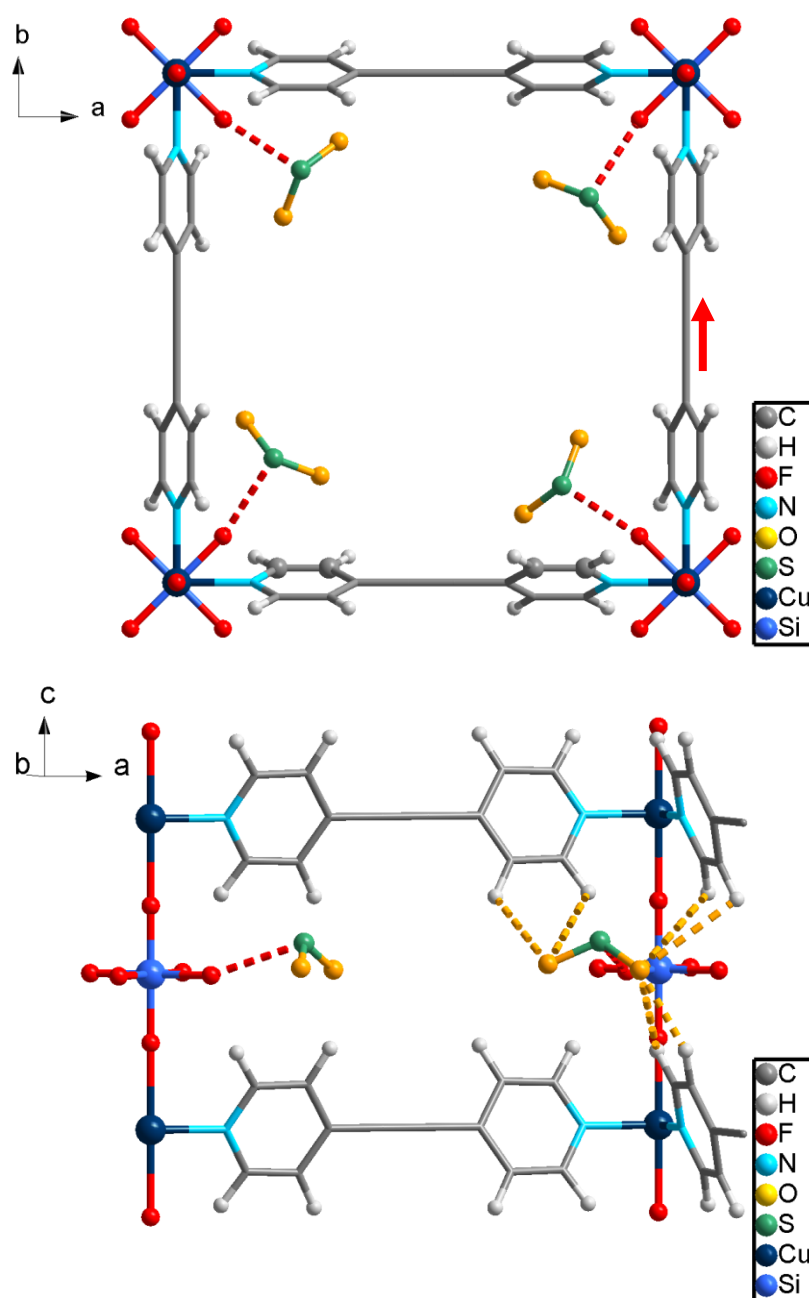


Figure S8 DFT-D simulated optimized SO₂ adsorption sites of SIFSIX-2-Cu in two different viewing directions (A and B).

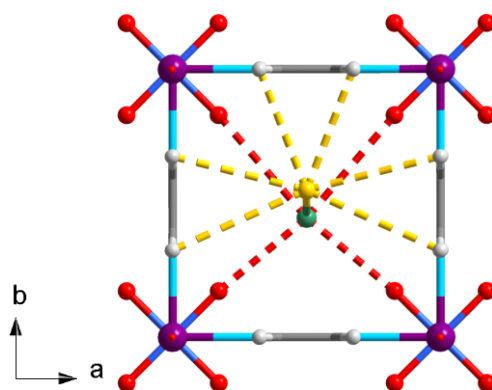


Figure S9 DFT-D simulated optimized SO_2 adsorption sites of SIFSIX-3-Zn viewed down the *c* axis.

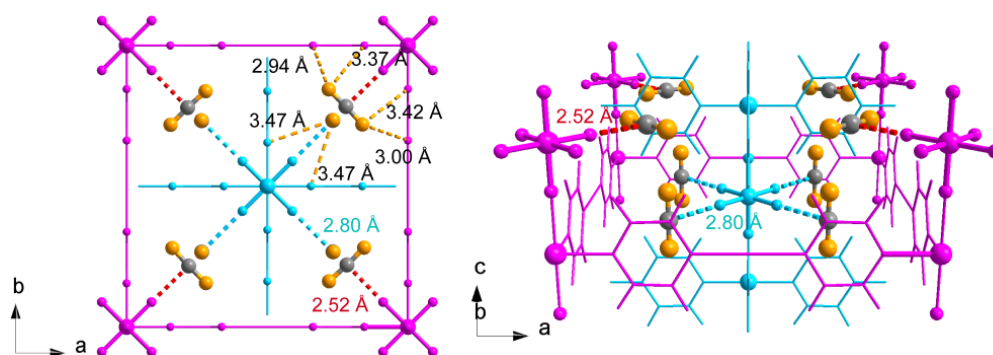


Figure S10. DFT-D calculated CO₂ adsorption sites in SIFSIX-2-Cu-i viewing in two different directions (A and B). (Note: the different nets are highlighted in magenta and cyan for clarity).

As shown in Figure S10, CO₂ were trapped in the interpenetrated SIFSIX-2-Cu-i through $C^{\delta+} \cdots F^{\delta-}$ and multiple $O^{\delta-} \cdots H^{\delta+}$ interactions. The DFT-D calculated distance of $C \cdots F$ from different nets are 2.80 and 2.52 Å, respectively (Figure S10). By contrast, the DFT-D calculated distance of $S \cdots F$ from different nets are both 2.44 Å, indicating much stronger electrostatic interactions between SO₂ and SIFSIX-2-Cu-i.

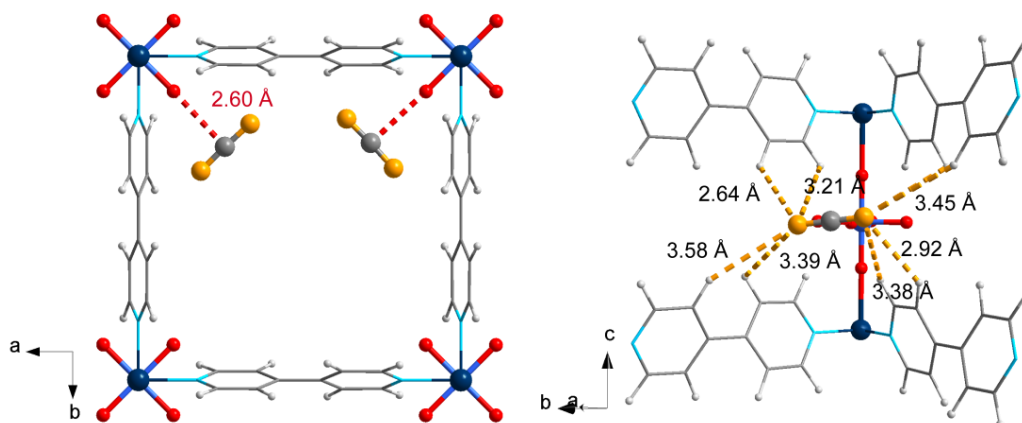


Figure S11. DFT-D calculated CO₂ binding sites in SIFSIX-1-Cu viewing in two different directions (A and B). Colour code: F, red; Si, light blue; C, grey; H, light grey; N, sky blue; Cu, dark teal; O, orange.

In SIFSIX-1-Cu, the adsorbed CO₂ are bound by the $C^{\delta+} \cdots F^{\delta-}$ (Figure S11A) and multiple $O^{\delta-} \cdots H^{\delta+}$ (Figure S11B) interactions. The DFT-D calculated distance of $C \cdots F$ (2.60 Å) is comparable to the calculated distance of $S \cdots F$ is 2.61 Å. And the DFT-D calculated O \cdots H distance of CO₂ molecule with 4,4'-bipyridine ranged from 2.64 ~ 3.58 Å, longer than the O \cdots H distance of SO₂ molecule with 4,4'-bipyridine (2.39~3.30 Å). These multiple interactions shows a stronger interactions between SO₂ and SIFSIX-1-Cu.

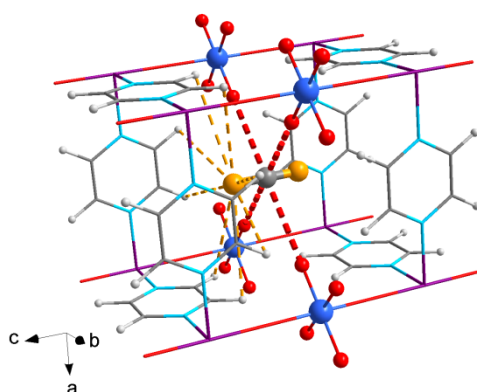


Figure S12. DFT-D calculated CO₂ binding sites in SIFSIX-3-Zn. Colour code: F, red; Si, light blue; C, grey; H, light grey; N, sky blue; Zn, violet; O, orange.

With a small pore size of SIFSIX-3-Zn, CO₂ were captured through four cooperative C^{δ+}...F^{δ-} and multiple O^{δ-}...H^{δ+} interactions. Adsorbed at the center of the one-dimensional channel (Figure S12), all of the four C...F distance were 3.36 Å.

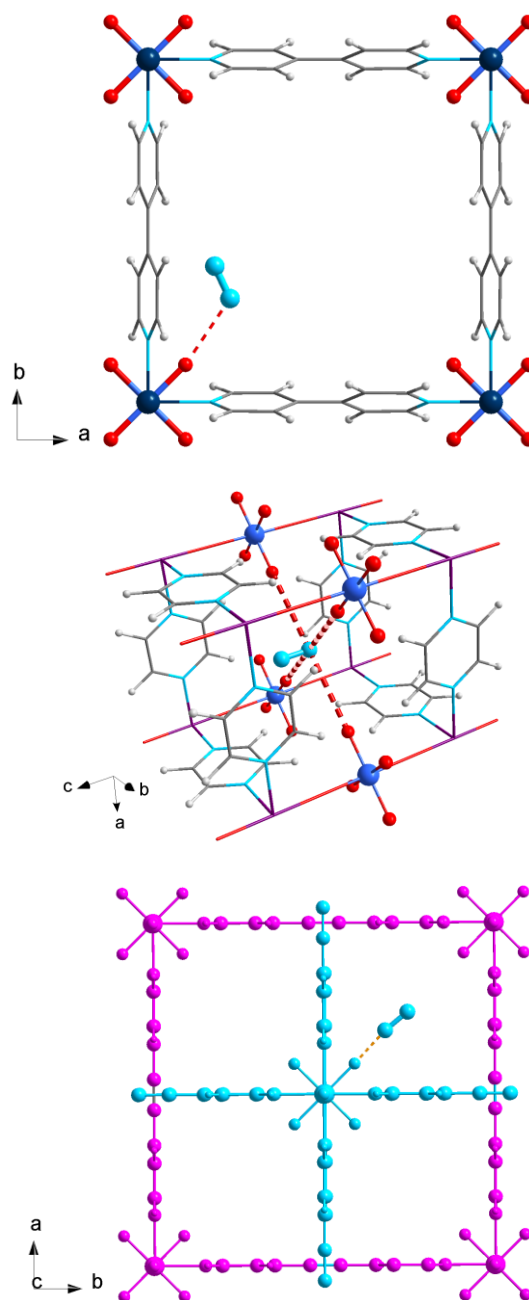


Figure S13. DFT-D calculated N_2 adsorption sites in SIFSIX-1-Cu (A), SIFSIX-3-Zn (B), and SIFSIX-2-Cu-i (C). Colour code: F, red; Si, light blue; C, grey; H, light grey; N, sky blue; Cu, dark teal; Zn, violet; O, orange. (Note: the different nets of SIFSIX-2-Cu-i are highlighted in magenta and cyan for clarity).

In addition, the calculated adsorption energy (ΔE) shows that there are much stronger interactions with SO_2 than CO_2 (ΔE in SIFSIX-2-Cu-i, 50.2 versus 35.7 kJ mol^{-1} ; ΔE in SIFSIX-1-Cu, 50.3 versus 31.1 kJ mol^{-1} ; ΔE in SIFSIX-3-Zn, 54.1 versus 45.7 kJ mol^{-1}). As for N_2 , the calculated ΔE also shows that there are much stronger interactions with SO_2 than N_2 (ΔE in SIFSIX-2-Cu-i, 50.2 versus 22.8 kJ mol^{-1} ; ΔE in SIFSIX-1-Cu, 50.3 versus 15.7 kJ mol^{-1} ; ΔE in SIFSIX-3-Zn, 54.1 versus 25.2 kJ mol^{-1}).

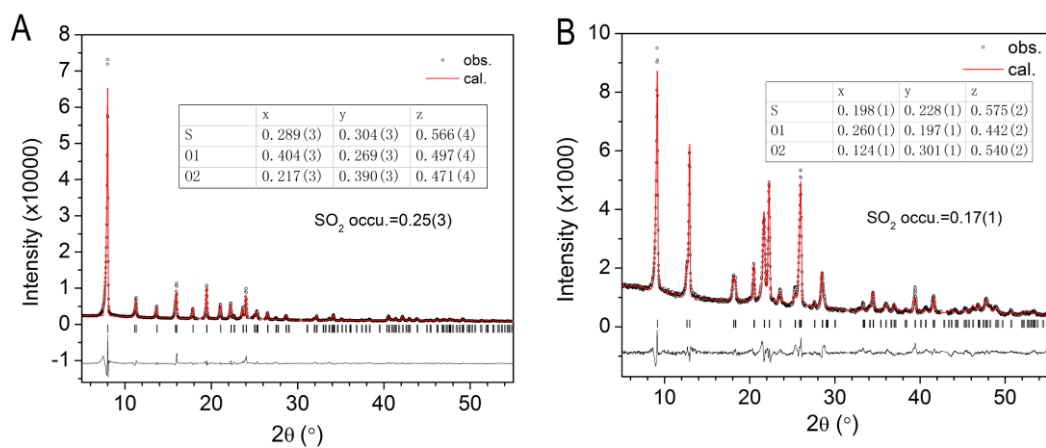


Figure S14. Powder X-ray diffraction patterns for the Rietveld refinement of SO₂-loaded SIFSIX-1-Cu (A) and SO₂-loaded SIFSIX-2-Cu-i (B). Goodness of fit data: (A) $R_{wp} = 0.0891$, $R_p = 0.0624$, $\chi^2 = 3.96$; (B) $R_{wp} = 0.0666$, $R_p = 0.0492$, $\chi^2 = 1.99$.

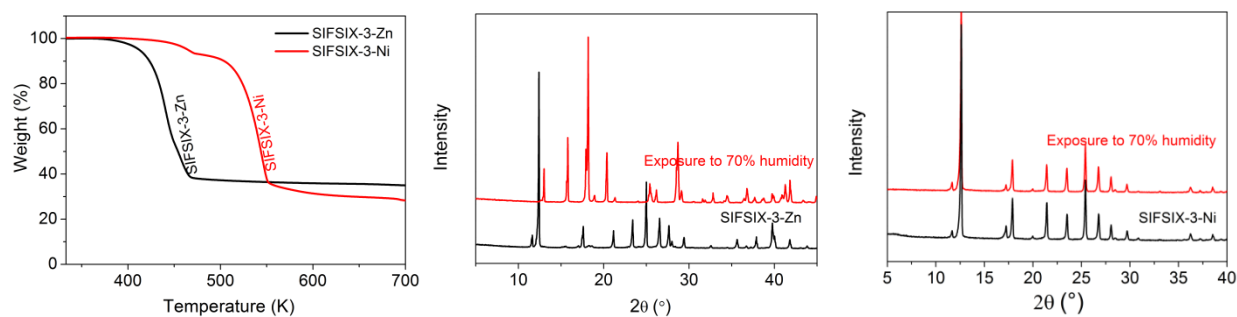


Figure S15. TGA patterns of sample SIFSIX-3-Zn and SIFSIX-3-Ni (A). XRD patterns of sample SIFSIX-3-Zn (B) and SIFSIX-3-Ni (C) after exposure to 75% humidity for 1 day.

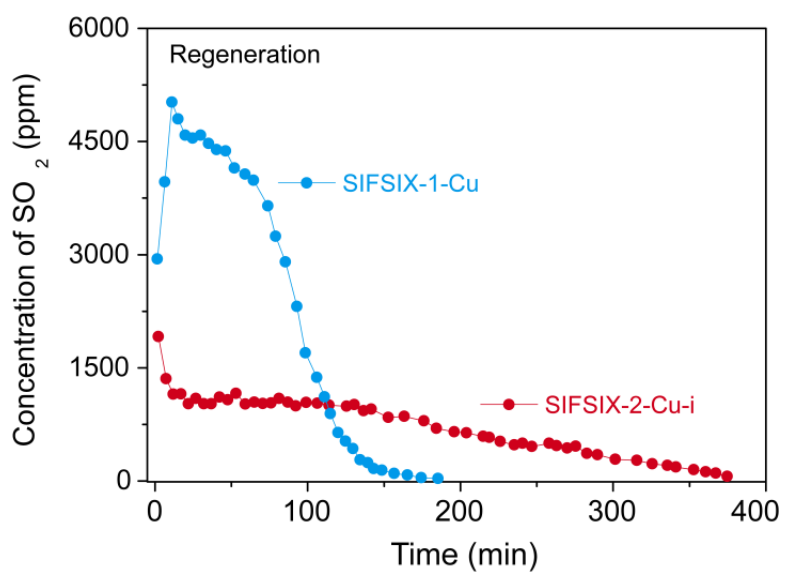


Figure S16. Experimental desorption curves for SO₂ on SIFSIX-2-Cu-i ($\Phi 4.6 \times 50$ mm, 0.21 g) and SIFSIX-1-Cu ($\Phi 4.6 \times 50$ mm, 0.23 g) with He flow of 20 ml min⁻¹ at 313 K.

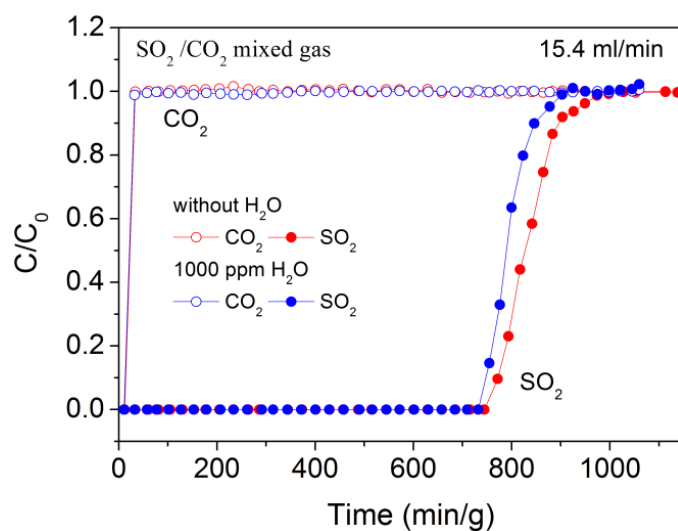


Figure S17. Experimental column breakthrough curves for SO₂/CO₂ separations on SIFSIX-2-Cu-i (Φ4.6×50 mm, 0.21 g) at 298 K and 1.01 bar with the presence of moisture. The composition of the mixed gas: 1000 ppm H₂O, 1870 ppm SO₂, and 99.713% CO₂.

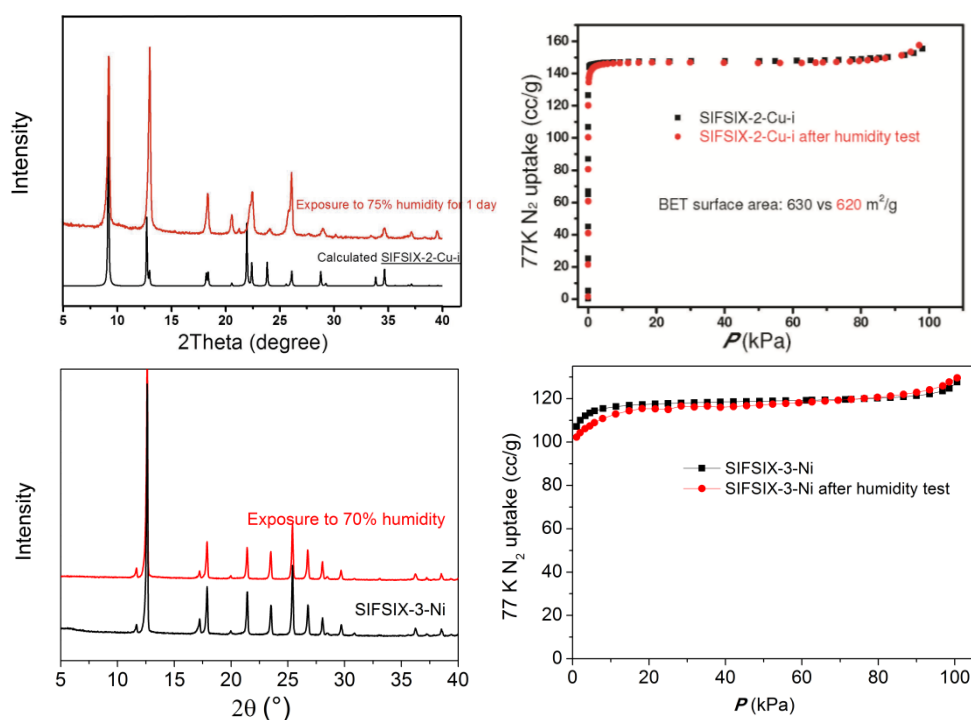


Figure S18. XRD patterns of sample SIFSIX-2-Cu-i after exposure to 75% humidity for 1 day (A). The BET curves of fresh SIFSIX-2-Cu-i and the sample after exposure to 75% humidity for 1 day (B). XRD patterns of sample SIFSIX-3-Ni after exposure to 70% humidity for 5 days (C). The BET curves of fresh SIFSIX-3-Ni and the sample after exposure to 70% humidity for 5 days (D).^[6]

Reference

- [1] S.-I. Noro, R. Kitaura, M. Kondo, S. Kitagawa, T. Ishii, H. Matsuzaka, M. Yamashita, *J. Am. Chem. Soc.* **2002**, 124, 2569.
- [2] P. Nugent, Y. Belmabkhout, S. D. Burd, A. J. Cairns, R. Luebke, K. Forrest, T. Pham, S. Q. Ma, B. Space, L. Wojtas, M. Eddaoudi, M. J. Zaworotko, *Nature* **2013**, 495, 80.
- [3] A. Kumar, D. G. Madden, M. Lusi, K.-J. Chen, E. A. Daniels, T. Curtin, J. J. Perry IV, M. J. Zaworotko, *Angew. Chem. Int. Ed.* **2015**, 54, 14372.
- [4] X. Cui, K. Chen, H. Xing, Q. Yang, R. Krishna, Z. Bao, H. Wu, W. Zhou, X. Dong, Y. Han, B. Li, Q. Ren, M. J. Zaworotko, B. Chen, *Science* **2016**, 353, 141.
- [5] V. Barone, M. Casarin, D. Forrer, M. Pavone, M. Sambri, A. Vittadini, Role and effective treatment of dispersive forces in materials: polyethylene and graphite crystals as test cases, *Comput. Chem.* **2009**, 30, 934.
- [6] X. Cui, K. Chen, H. Xing, Q. Yang, R. Krishna, Z. Bao, H. Wu, W. Zhou, X. Dong, Y. Han, B. Li, Q. Ren, M. J. Zaworotko, B. Chen, *Science* **2016**, 353, 141.